



# The push and pull of abandoned channels: How floodplain processes and healing affect avulsion dynamics and alluvial landscape evolution in foreland basins

Harrison K. Martin<sup>1</sup>, Douglas A. Edmonds<sup>1</sup>

5 <sup>1</sup>Department of Earth and Atmospheric Sciences, Indiana University, Bloomington, Indiana, 47408, United States of America

*Correspondence to:* Harrison K. Martin (hkmartin@iu.edu)

## Abstract

River avulsions are an important mechanism by which sediment is routed and emplaced in foreland basins. However, because avulsions occur infrequently, we lack observational data that might inform where, when, and why avulsions occur and these questions are instead often investigated by rule-based numerical models. These models have historically simplified or neglected the effects of abandoned channels on avulsion dynamics, even though fluvial megafans in foreland basins are characteristically covered in abandoned channels. Here, we investigate the pervasiveness of abandoned channels on modern fluvial megafan surfaces. Then, we present a physically based cellular model that parameterizes interactions between a single avulsing river and abandoned channels in a foreland basin setting. We investigate how abandoned channels affect avulsion set-up, pathfinding, and landscape evolution. We demonstrate and discuss how the processes of abandoned channel inheritance and transient knickpoint propagation post-avulsion serve to shortcut the time necessary to set-up successive avulsions. Then, we address the idea that abandoned channels can both repel and attract future pathfinding flows under different conditions. By measuring the distance between the mountain-front and each avulsion over long ( $10^6$  to  $10^7$  years) timescales, we show that increasing abandoned channel repulsion serves to push avulsions farther from the mountain-front, while increasing attraction pulls avulsions proximally. Abandoned channels do not persist forever, and we test possible channel healing scenarios (deposition-only, erosion-only, and far-field directed) and show that only the final scenario achieves dynamic equilibrium without completely filling accommodation space. We also observe megafan growth occurring via  $\sim 10^5$  year lobe switching, but only in our runs that employ deposition-only or erosion-only healing modes. Finally, we highlight opportunities for future field work and remote sensing efforts to inform our understanding of the role that floodplain topography, including abandoned channels, plays on avulsion dynamics.

10  
15  
20  
25

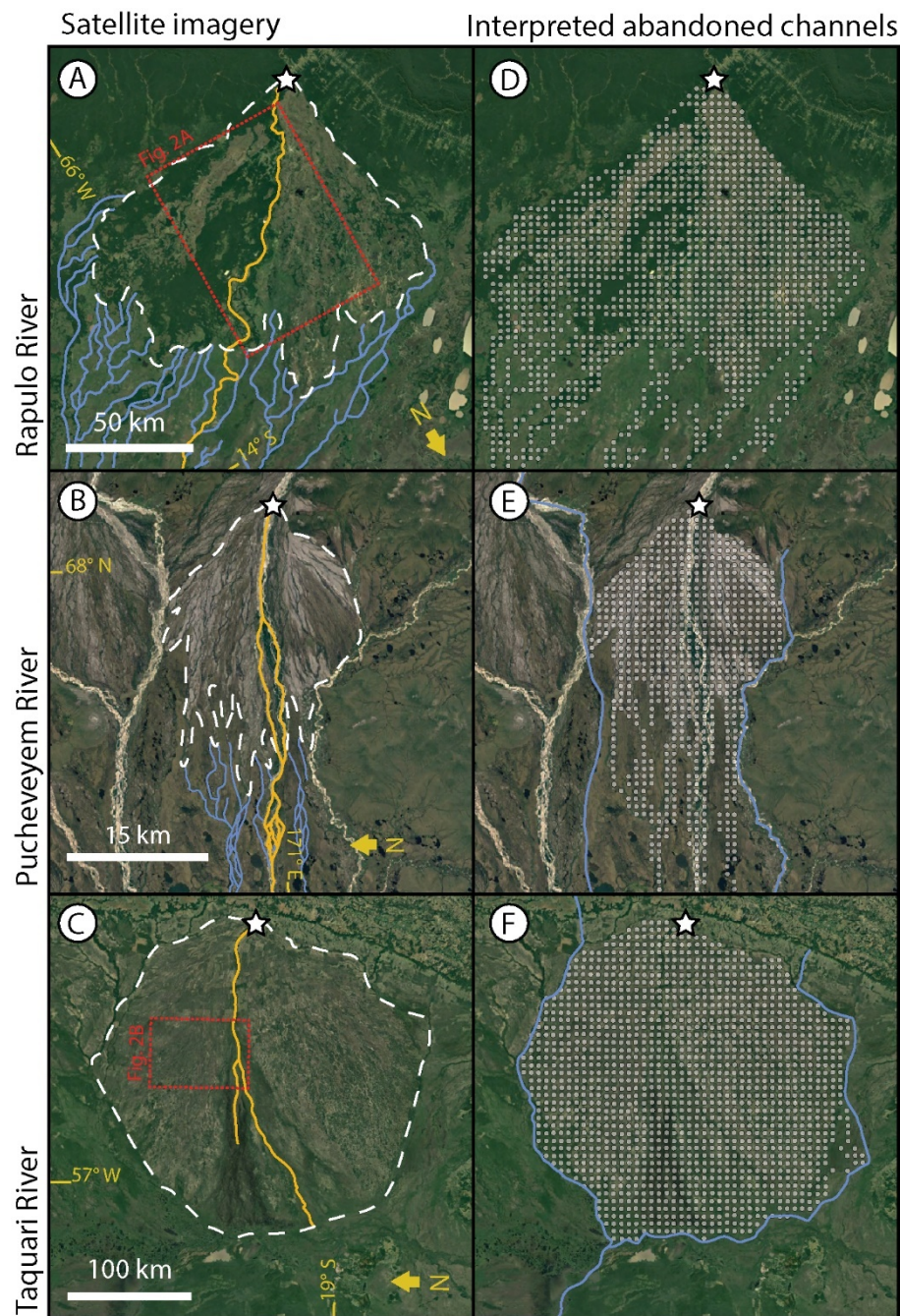


## 1 Introduction

Avulsions, the wholesale relocations of rivers into new positions on their floodplains, are a primary control on how water and sediment are routed through alluvial landscapes (Mackey and Bridge, 1995). The predominant conceptual model presents avulsions as requiring two necessary components: a set-up, and a triggering event that causes bank failure and avulsion (Slingerland and Smith, 2004). However, there is a lack of observational data on each of these necessary components because avulsions occur infrequently (Edmonds et al., 2016). Instead, avulsion dynamics are often explored using concept-driven numerical models. One such form is cellular models, which seek to reduce the system to the components necessary to reproduce a natural phenomenon (Jerolmack and Paola, 2007). For planform avulsion models, this usually entails some description of sediment transport and deposition along an active channel and associated floodplain, and semi-heuristic rules for how avulsions are set-up, initiate, and pathfind (Hajek and Wolinsky, 2012). However, models have historically simplified or neglected the effect of abandoned channels on avulsion dynamics (Pelletier et al., 2005; Reitz et al., 2010). The relict topographic highs and lows associated with alluvial ridges, levees, and abandoned channels should affect both avulsion set-up and avulsion pathfinding by repelling or attracting flows (Leeder, 1977; Allen, 1978; Jerolmack and Paola, 2007; Reitz et al., 2010).

The large, fan-shaped, low-relief fluvial megafans that exist where rivers leave lateral confinement and enter foreland basins are ideal locations to study the interaction between avulsions and abandoned channels (Fig. 1A; Leier et al., 2005; Weissmann et al., 2010). Fluvial megafans have some of the highest avulsion rates in the observational record (Valenza et al., 2020) and, in contrast to deltaic fans, have been qualitatively described as hosting abundant abandoned channels (e.g., Assine and Soares, 2004; Rossetti and Valeriano, 2007; Chakraborty et al., 2010; Bernal et al., 2011; Weissmann et al., 2013). However, we lack a detailed evaluation of the prevalence or distribution of this channelization, which is important to understand the degree to which avulsions may interact with abandoned channels.

In this paper, we present observational data on the channelization of fluvial megafan surfaces in alluvial foreland basin settings and we use these observations to motivate a physically based numerical model that parameterizes interactions between an avulsing river and abandoned channels in a subsiding basin. Our model implements tuneable abandoned channel dynamics that influence how abandoned channels affect pathfinding and are removed from the floodplain. Incorporating abandoned channel floodplain dynamics allows us to assess how abandoned channels affect where, when, and why avulsions occur. We demonstrate that abandoned channels, their interactions with future pathfinding flows, and the way they are removed from the floodplain are all important controls on avulsion locations, dynamics, and resulting foreland basin deposition and geomorphology that should be considered in future models and studies.



55 Figure 1: (a-c) Remote sensing images and (d-f) abandoned channel maps for three fluvial megafans. The fans are located along the  
Rapulo River in Bolivia (a,d), the Pucheveyem River in Russia (b,e), and the Taquari River in Brazil (c,f). Note the downstream  
transition between distributive, densely channelized abandoned channel networks to tributive, sparsely channelized networks.  
Dashed white lines in (a-c) are interpreted megafan boundaries (see text for details), and white stars mark megafan apices. Blue lines  
in (a-c) show interpreted abandoned channel pathways outside of the megafan boundary. Solid gold lines show active channels. All  
60 satellite images are USGS/NASA Landsat/Copernicus, © Google Earth.



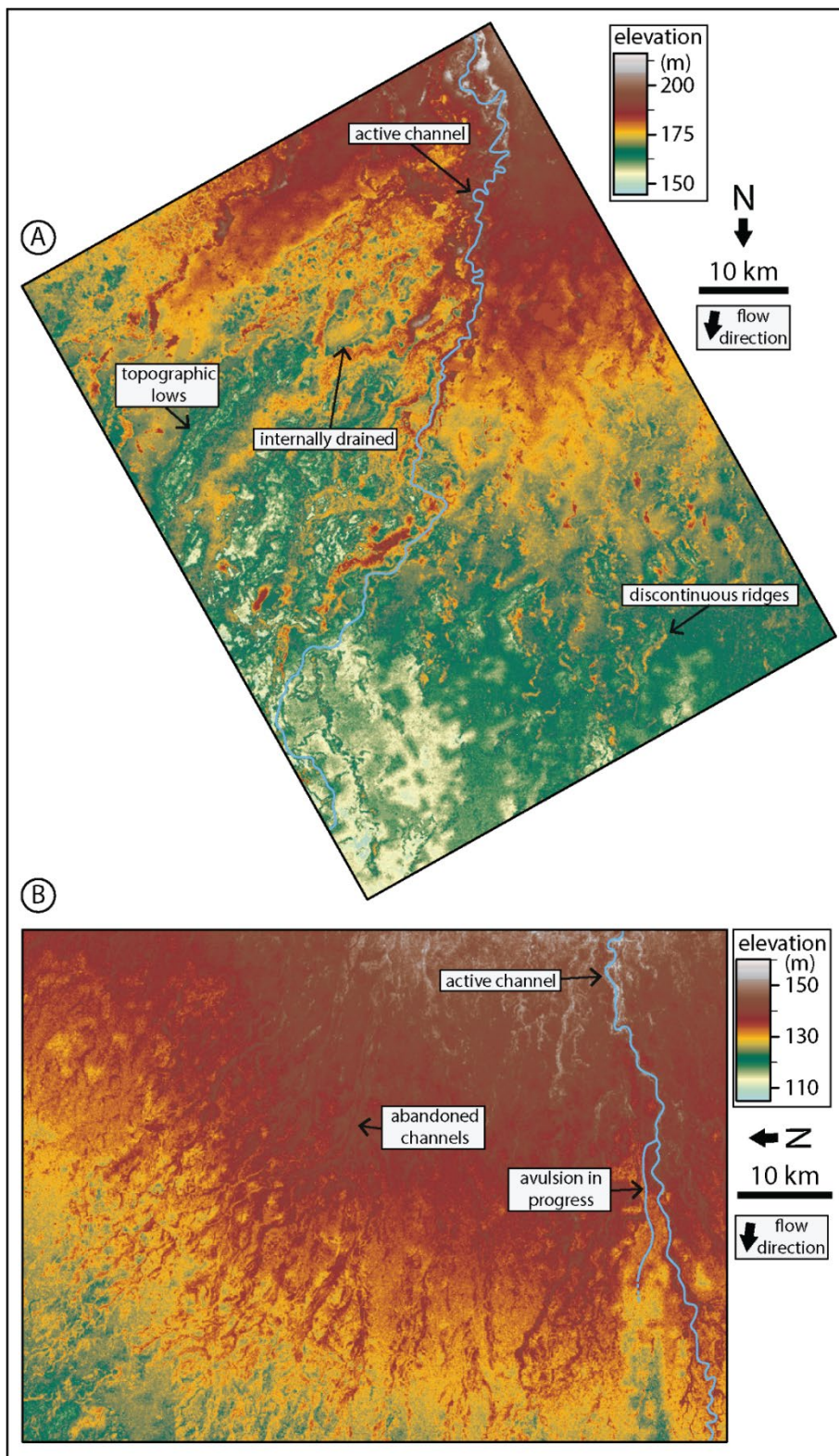
## 2. Observations of modern fluvial megafan surfaces

We created maps of abandoned channels on a non-exhaustive set of three megafans (Fig. 1) that represents a range of megafan sizes and settings with typical appearances (Hartley et al., 2010a; Weissmann et al., 2010), and that includes the well-studied Taquari megafan (e.g., Assine, 2005; Makaske et al., 2012; Zani et al., 2012). Following previous work (Rossetti and Valeriano, 2007; Bernal et al., 2011), we combine Google Earth, Landsat visual imagery, and bare-earth topography to identify abandoned channels on South American megafans. For elevation data, we use the BEST (Bare-Earth Srtm Terrain) elevation model, which uses vegetation maps and satellite lidar to reveal bare-earth topography by correcting for vegetation elevations present in radar-derived topography (O'Loughlin et al., 2016; Moudrý et al., 2018). On top of each megafan, we overlaid a rasterized grid with square cells with dimensions that corresponded to roughly five channel widths, similar to the resolution of the cellular model that is described later. Within each cell we marked whether there was topographic or visual evidence of abandoned channels (Fig. 1B). Evidence of abandoned channels consisted of identified channelized features with long axes generally oriented toward the apex of the fan, with widths approximately equal to the active channels on the fan. Abandoned channels were usually visible in satellite imagery, but in areas with dense tree canopies, we looked for channel-like pathways delineated by differences in coloration against the adjacent floodplain. These differences result from the historical presence of an active channel (Bernal et al., 2011); abandoned channels may have coloration that is lighter (due to sediment emplacement; Valenza et al., 2020) or darker (due to increased vegetative density associated with additional standing or groundwater). Where possible, we used the topographic data in tandem with the visual data to confirm that a cell contained an abandoned channel.

### 2.1. Remote sensing results:

These three fluvial megafans have abundant abandoned channels within their boundaries (Fig. 1). Megafan boundaries were drawn to encapsulate regions of positive relief and greater slope relative to the surrounding basin (Fig. 1A-C). Within these boundaries, between 95% (Rapulo) and >99% (Pucheveyem and Taquari) of cells on megafan surfaces contained interpreted abandoned channel features. Downstream of the megafan boundary there is a transition from distributive to tributive planform morphologies (Fig. 1A,B), wherever they are not bounded by topography or an axial river (Fig. 1C; cf. methodology of Hartley et al., 2010a). In contrast to other distributary fan systems like alluvial fans or some deltas, within the fan we usually observed a single active channel with one or multiple threads and occasional bifurcation (Hartley et al., 2010a). This suggests that, rather than hosting many contemporaneous distributary channels, the distributive nature of megafans arises over time through repeated avulsions along a small number of active channels (Weissmann et al., 2010).







90 **Figure 2: Bare-earth digital elevation models (O’Loughlin et al., 2016) of floodplain topography on the Rapulo (a) and Taquari (b) megafans. Locations are in Fig. 1. Floodplains are densely channelized by abandoned channels with visible topographic highs and lows corresponding to levees or alluvial ridges and channel beds, respectively. Note the presence of discontinuous alluvial ridges.**

We observed that abandoned channels can be both topographic highs (associated with levees or alluvial ridges) and topographic lows (associated with abandoned channels that have not been fully in-filled with sediment) relative to surrounding floodplains (Fig. 2). In some portions of the fan there were ‘internally drained’ areas surrounded by topographic abandoned channel highs (Fig. 2A). These abandoned alluvial ridges were not necessarily spatially continuous in the downstream direction, often forming discontinuous ridges (Fig. 2; Rossetti and Valeriano, 2007). The topographic data were collected during an ongoing avulsion on the Taquari fan, and the avulsion location is immediately adjacent to a topographic low on its floodplain (Buehler et al., 2011). Multiple avulsions on the Rapulo megafan during the Landsat observation period have also initiated into local topographic lows adjacent to the channel (Edmonds et al., 2021).

## 100 2.2. Megafan floodplain topography discussion:

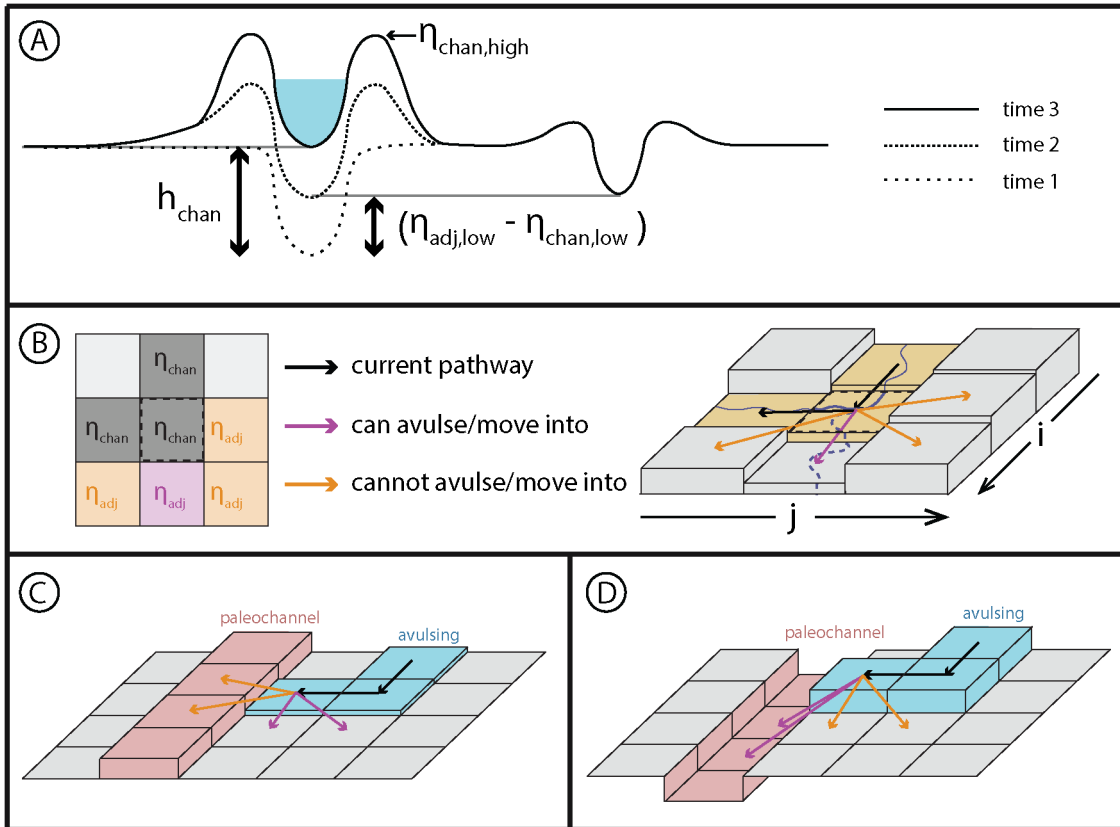
The degree of floodplain channelization observed and interpreted in Fig. 1 and Fig. 2 suggests that avulsions would be influenced by abandoned channels. Following this, we envision at least two aspects of avulsion dynamics that can be influenced by the presence of abandoned channels and can be easily incorporated into a model.

### 2.2.1 Avulsion set-up & initiation

105 The most common conception of avulsion set-up is superelevation, whereby in-channel deposition outpaces deposition in the surrounding floodplain, leading to a perched channel that transports water and sediment less efficiently than some novel path on the floodplain (Bryant et al., 1995; Slingerland and Smith, 2004). On a flat, featureless floodplain with a channel that can counter-act subsidence exactly, the time to achieve superelevation ( $T_A$ , years) for some arbitrary point along a river is commonly (e.g., Jerolmack and Mohrig, 2007; Jerolmack, 2009; Martin et al., 2009; Reitz et al., 2010; Moodie et al., 110 2019) approximated as

$$T_A = \frac{\beta * h_{chan}}{(A_{chan} + \sigma) - A_{fp,tot}} \quad (1)$$

where  $\beta$  is a non-dimensional channel depth fraction (generally assumed to be 0.5-1.0; Mohrig et al., 2000),  $h_{chan}$  is the channel depth (meters) at a particular point in the river,  $A_{chan}$  is the in-channel-bed aggradation rate (meters per year),  $A_{fp,tot}$  is the total floodplain aggradation rate (meters per year) and  $\sigma$  is the subsidence rate (meters per year; positive in the downwards direction). Conceptually, this superelevation timescale is equal to the time necessary for the channel bed to aggrade some specified fraction of a channel depth (Fig. 3A).



125 Abandoned channels on the floodplain can short-circuit this timescale by reducing the amount of aggradation needed  
 to superelevate (Fig. 3A). If an abandoned channel is close to the active one, then this should encourage avulsion because  
 during high flow there would be a steep water surface gradient that would cause erosion of the intervening levee and reroute  
 the flow. This requires that the abandoned channel is roughly the same size as the active one and that it is close enough to  
 increase the water surface gradient. What constitutes ‘close enough’ is unknown, though the Taquari avulsion is observed to  
 130 proceed into an adjacent topographic low (Fig. 2B), as are repeated avulsions along the Rapulo river (Edmonds et al., 2021).  
 In effect, the lower elevation of the abandoned channel bed relative to its surrounding floodplain reduces the amount of  
 aggradation needed for superlevation. We can thus rewrite the superlevation timescale of Eq. (1) as

$$T_A = \frac{\beta * (\eta_{adj,low} - \eta_{chan,low})}{(A_{chan} + \sigma) - A_{fp,tot}}, \text{ for } \eta_{adj,low} > \eta_{chan,low} \quad (2)$$



where  $\eta_{chan,low}$  and  $\eta_{adj,low}$  represent the elevations (meters) of the active channel bed and the area adjacent to the channel, respectively (Fig. 3B). This adjacent elevation can vary based on the topography adjacent to the channel. For example, if there is an abandoned channel bed that is inset into the surrounding floodplain adjacent to the river, then  $(\eta_{chan,low} - \eta_{adj,low}) < h_{chan}$ , and Eq. (2) will result in a shorter avulsion set-up timescale than would be expected for a featureless floodplain (Eq. (1); Mohrig et al., 2000). Even though this is a simple amendment to Eq. (1), as we show later it has important effects on avulsion timing and location.

Channel reoccupation could also shorten superelevation timescales. Given the density of channels we observed on megafans (Fig. 1; Fig. 2), it seems that reoccupation must be common (Valenza et al., 2020). When active channels avulse, any previous aggradation downstream of the avulsion locus is not immediately destroyed. Instead, if these channels are later reoccupied, and had not been completely scoured out in the interim, then Eq. (2) allows for superelevation to be inherited. In these two ways, abandoned channels can cause rivers to have avulsion set-up timescales that are much less than via relative aggradation or subsidence alone as embodied in Eq. (1).

### 2.2.2 Avulsion pathfinding

Abandoned channels are so prevalent on fan surfaces that they should also affect avulsion pathfinding (Fig. 1; Fig. 2; Edmonds et al., 2016; Valenza et al., 2020). Despite this, most previous models have assumed abandoned channels have no effect on future avulsion pathfinding (Leeder, 1977; Ratliff et al., 2018), or act as universal repulsors (Allen, 1978; Bridge and Leeder, 1979) or universal attractors (Jerolmack and Paola, 2007; Reitz et al., 2010). The reality seems to be somewhere in-between these endmembers. After all, if abandoned channels retain superelevation that once drove avulsion and abandonment, then that superelevation would topographically repel later pathfinding events (Leeder, 1977; Allen, 1978; Fig. 3C). We observe both topographic lows and highs on modern megafans, including discontinuous alluvial ridges (Fig. 2). This suggests that abandoned channels can be both attractive and repulsive at different locations and times on the fan surface (Allen, 1978). This is consistent with recent observations that suggest avulsions are pushed away from their parent channels by alluvial ridges but inevitably attracted back into a channel some distance downstream (Edmonds et al., 2016; Valenza et al., 2020). Importantly, attraction seems to be a near universal behavior; all 63 avulsions identified by Valenza et al. (2020) experienced some reoccupation.

In addition to affecting avulsion dynamics, the rate at which these abandoned channels (and associated alluvial ridges and scours) are removed should affect landscape evolution because abandoned channels contribute much or most of the topography on modern megafans (Fig. 2). There are virtually no observations of abandoned channel healing rates, and as such it is unclear in models whether to treat abandoned channels as healing instantly, persisting indefinitely, or some intermediary. Additionally, if one assumes that abandoned channels do heal, the mode of abandoned channel healing is unclear; while preferential deposition in abandoned channel topographic lows ('bottom-up' healing) is known to occur in at least some abandoned channels (Schmudde, 1963; Toonen et al., 2012), the relative degree of levee erosion ('top-down' healing) is





unknown. Top-down healing is plausible if a combination of diffusive sediment transport, weathering, and fluvial erosion during floods erode topographic highs on the floodplain (Hack and Goodlett, 1960; Burkham, 1972; Zwoliński, 1992; Gabet, 2000; Croke et al., 2013). See Sect. 5.2 in the Discussion for more details. In summary, however, there are unanswered questions about the fates and rates of abandoned channel floodplain topography. These questions have important implications for the gross morphology of foreland basins and their deposits because the primary mode of sediment transport and emplacement in this depositional environment is via alluvium deposited by and between avulsions.

### 3. Model conception and implementation

#### 3.1 Model overview & routine

The prevalent channelization of fluvial megafan surfaces led us to consider how abandoned channels may affect avulsion dynamics and landscape evolution in foreland basin settings. To test these effects, we created a physically based cellular model of an evolving alluvial landscape with parameterized and tuneable abandoned channel dynamics ('RiverWalk'; available at DOI:10.5281/zenodo.5576789). Our model is intentionally simplified as much as possible while retaining the ability to recreate the essential features of fluvial megafans in foreland basins (Bokulich, 2013). As a brief conceptual overview, our model consists of a single river exiting a mountain-front and transporting some fixed amount of water discharge and sediment flux. As it enters a foreland basin, relative subsidence causes sediment to be deposited preferentially near the mountain-front. This leads to river avulsion via superelevation, and over time these avulsions construct a radially oriented fan through the emplacement of channels that individually aggrade before abandonment. In our model, these abandoned channels can affect avulsion dynamics. For simplicity, we ignore the impacts of other rivers or fans and of any other mountain-front processes that may advect sediment into the basin.

The model routine operates as follows; more details on individual components are provided in Tables 1 and 2 and in the sections that follow. We paired a 1D diffusive channel-bed-elevation model (Paola et al., 1992) that describes how elevation in a river channel diffuses due to sediment transport with a rectangular, 2D cellular computational domain of 150 km per side that describes the floodplain and surrounding basin. Following Jerolmack and Paola (2007), each cell has a low (channel-bed) and high (levee or alluvial ridge) elevation. The simulation initializes by assuming the channel takes a straight path to the bottom of the domain (Table 1). The 1D sediment transport model is calculated to equilibrium along this path (Table 1). This profile is then replicated along strike to populate floodplain cells. This creates an underfed basin because nearly all subsequent river paths will be longer than a straight line, which causes aggradation and avulsion.



**Table 1: Non-experimental avulsion model parameters**

Parameter	Value
Timestep	10 yr
Grid Dimensions	301 cells x 301 cells
Cell Size	500 m x 500 m
Random Walk Weights	In descending order of steepness: 40%, 27.5%, 17.5%, 10%, and 5%.
Minimum Superelevation ( $\beta$ <i>sensu</i> Mohrig et al., 2000.)	Channel-base equal to neighboring floodplain cell ( $\beta = 1$ )
Overbank Aggradation (Fixed-Rate Component)	Proximal: $1 \times 10^{-7}$ m/yr Distal: $2.5 \times 10^{-6}$ m/yr
Subsidence Rate (linearly interpolated)	Proximal: $1 \times 10^{-5}$ m/yr Distal: $5 \times 10^{-6}$ m/yr
Initialization Apex Elevation	Variable; ~5-10% less than final apex elevation; see Table 3.

195

After the first avulsion, a new river pathway is established within a single timestep from the avulsion point (Sect. 3.3.1) and is set into the domain one channel depth below the surface. The pathway is selected via steepness-weighted random walk to any point along the bottom boundary of the domain (Sect. 3.3.1), and all floodplain cells along this path are converted to active channel cells (Sect. 3.3). The timestep increments and the elevations of each cell along the new pathway are transiently diffused to represent river adjustment (Sect. 3.3). At the upstream boundary of the diffusion model, water and sediment come in at a fixed rate so that the surface slope does not change (Table 2), and at the downstream boundary the elevation is fixed at 0 m. Diffusion continues until an avulsion trigger (with a fixed probability at each timestep) occurs and avulsion criteria (superelevation and gradient advantage) are satisfied for at least one active channel cell (Sect. 3.3.1). The avulsion location is randomly selected from among viable cells and pathfinding proceeds as before, but now the river can be repelled or attracted (i.e., captured) by abandoned channels. Pathfinding stops when the avulsion is successful and encounters the bottom boundary, or when the avulsion fails after becoming terminally trapped (Sect. 3.3.1). In both situations the timestep is incremented, but in the successful case any active channel cells that are no longer occupied become abandoned channel cells, and in the failure case the domain is restored to its pre-avulsion state.

205



210 **Table 2: Sediment diffusion calculation parameters**

Parameter	Value
Initial Specific Discharge (apex)	$1.9 \times 10^5 \text{ m}^2/\text{yr}$
Incoming Sediment Supply	$400 \text{ m}^3/\text{yr}$
Basin Width (for discharge calculation)	$5 \times 10^4 \text{ m}$
Coefficient $A$	1.00
Nondimensional coefficient of friction	0.01
$C_0$	0.7
$S$	1.65
$\rho_{\text{sediment}}$	$2.65 \times 10^3 \text{ kg m}^{-3}$
$\rho_{\text{water}}$	$1.00 \times 10^3 \text{ kg m}^{-3}$

In all future timesteps, after updating the 2D landscape and before checking for avulsion triggers, floodplain and abandoned channel processes routines are executed. First, all non-active channel cells experience subsidence at a rate that decreases away from the mountain front (representing a foreland basin) and overbank floodplain deposition that varies with distance from the mountain front but not with distance from the channel (Sect. 3.3.2). Next, abandoned channels are healed by a steady-rate topographic adjustment function until they reach a specified healing endpoint (3.3.2). Finally, any abandoned channel cells with less than 25% of a mean channel depth in remnant relief are converted to floodplain cells (Sect. 3.3).

### 3.2 1D diffusive channel-bed elevation model

The 1D model has a variable length that is equal to that of the planform river pathway established in the 2D model. We used transient diffusion to model channel-bed elevation changes along this pathway that would occur from sediment transport (Paola et al., 1992):

$$\sigma + \frac{\partial \eta_{\text{chan,low}}}{\partial t} = \frac{\partial}{\partial x} \left( v \frac{\partial \eta_{\text{chan,low}}}{\partial x} \right), \quad v = -\frac{8qA\sqrt{c_f}}{C_0(S-1)} \quad (3)$$

where  $t$  is time (years),  $x$  is space (meters),  $v$  is diffusivity (square meters per year),  $q$  is normalized water discharge per unit basin width (square meters per year),  $A$  is a non-dimensional constant set to 1,  $c_f$  is a dimensionless drag coefficient,  $C_0$  is bed sediment concentration, and  $S$  is sediment specific gravity ( $\frac{\rho_{\text{sediment}} - \rho_{\text{water}}}{\rho_{\text{water}}}$ , non-dimensional; Table 2). We used the Crank-Nicolson solution scheme to solve this equation. This scheme is second-order, implicit in time, and unconditionally numerically stable for diffusion partial differential equations (Slingerland and Kump, 2011). Treating diffusion of the bed surface transiently (rather than bringing the river completely to equilibrium between each timestep [cf. Jerolmack and Paola, 2007]) allows for local aggradation or incision to occur on channel profiles out of equilibrium.



230 Our experimental design necessitated using nondimensional repulsion and attraction factors that are normalized to  
 channel depths. As such, it was necessary to determine channel depth ( $h_{chan}$ ) for each active channel cell. We solved for this  
 at every active channel cell once per timestep following Paola et al. (1992; Table 2). This method allows depth to vary as a  
 function of local slope. Immediately after avulsion, slope variations along channels can be extreme (Fig. 8). These extreme  
 variations in slope create unrealistic variations in depth over short distances. As such, when solving for channel depth, we  
 235 bound maximum and minimum slope to within a factor of two compared to the equilibrium profile.

### 3.3 2D cellular model: avulsions and floodplains

The computational domain is discretized into square cells of length 500 m. There are three types of cells in our model:  
 active channel ( $chan$ ), abandoned channel ( $aban$ ), and floodplain ( $fp$ ). All cells have two elevations ('high' and 'low') that we  
 track throughout each run. All elevations are measured in meters.

240 Active channel: Active channel cells represent the current pathway of the river. There is one contiguous pathway for  
 flow per timestep. We selected a cell size such that modeled rivers are approximately one fifth of the width of a cell; as a result,  
 channel-scale processes (like meandering, crevasse splays, or other lateral-distance-dependent depositional effects) are not  
 resolved.

The low elevation in each active channel cell represents the channel bed and is updated by transient diffusion as  
 245 described in Eq. (3). Then, high elevations are set to the greater of i) the high elevation at the last timestep, or ii) one channel  
 depth above the bed, such that:

$$(\eta_{chan,low})_t \text{ is given by Equation 3} \quad (4a)$$

$$(\eta_{chan,high})_t = \max \left\{ (\eta_{chan,high})_{t-1}, (\eta_{chan,low})_t + h_{chan} \right\} \quad (4b)$$

where  $t$  is the current timestep and  $t - 1$  is the prior one. This assumes that an aggrading river constructs levees that can  
 250 contain its flow depth, but levees are not lowered if the river incises.

Other cell types become active channel cells whenever they are occupied by the active channel after an avulsion.  
 During this process, the low elevations of the new channel pathway are inset one channel depth down from the high elevations  
 unless there is a channel that is already incised beyond this depth. This rule allows for channels to inherit levees (and  
 superelevation) and does not further erode abandoned channel cells that are already incised more than one channel depth below  
 255 their levees.

Abandoned channel: Abandoned channel cells include any cell that was once active but no longer contains water.  
 These cells are still capable of attracting and repulsing pathfinding avulsions. Each cell has low and high elevations that reflect  
 abandoned channel beds and levees, respectively. These elevations experience a linear healing rate that depends on healing  
 mode but ultimately adjusts the channel bed and levee elevations toward a specified endpoint (Sect. 3.3.2):

$$260 \quad \eta_{aban,low} = (\eta_{aban,low})_{t-1} + (A_{fp,tot} - \sigma) + H_{low} \quad (5a)$$





$$\eta_{aban,high} = (\eta_{aban,high})_{t-1} + (A_{fp,tot} - \sigma) + H_{high} \quad (5b)$$

where  $A_{fp,tot}$  is the total overbank aggradation rate on the floodplain (meters per year; Sect. 3.3.2), and  $H_{low}$  and  $H_{high}$  are the healing rates (meters per year) applied to the low and high elevations, respectively.

Abandoned channel cells can become active channel cells if they are later occupied after an avulsion. Otherwise, they will become floodplain cells when:

$$h_{aban} < (0.25 * \bar{h}) \quad (6a)$$

$$h_{aban} = (\eta_{aban,high} - \eta_{aban,low}) \quad (6b)$$

where  $\bar{h}$  is mean channel depth (meters) calculated over the entire length of the active channel at each timestep. While healing gradually lowers  $h_{aban}$ , there is no process that can increase this relief other than revisitation by the active channel, in which case the cells will become active channel cells.

**Floodplain:** Floodplain cells are those never been visited by a channel or have completely healed after visitation. High and low elevations are equal for floodplain cells except if they were once abandoned and have transitioned to floodplain (via the threshold in Eq. (11)) they maintain their unequal elevations until healing is complete. Floodplain cells do not repulse or attract pathfinding avulsions. However, their remnant (and possibly unequal) elevations do affect set-up and avulsion pathfinding via weighted random walk (Sect. 3.3.1).

Floodplain cells that retain any remnant relief are subjected to healing in the same manner as abandoned channel cells:

$$\eta_{fp,low} = (\eta_{fp,low})_{t-1} + (A_{fp,tot} - \sigma) + H_{low} \quad (7a)$$

$$\eta_{fp,high} = (\eta_{fp,high})_{t-1} + (A_{fp,tot} - \sigma) + H_{high} \quad (7b)$$

### 3.3.1 Avulsion processes:

**Avulsion set-up:** Avulsions occur via three steps: i) set-up, ii) initiation via triggering, and iii) floodplain pathfinding. Avulsion set-up (Slingerland and Smith, 2004) occurs from a combination of superelevation and flowpath gradient advantage. A cell is superelevated if the elevation of its channel-bed is equal to or greater than at least one of its five neighboring cells (not including the three upstream cells; Fig. 3A,B) by some fraction of a mean channel depth:

$$(\eta_{chan,low} - \eta_{adj,low}) \geq (\beta - 1) * \bar{h} \quad (8)$$

We set  $\beta = 1$ , which requires the active channel bed to meet or exceed an adjacent cell's low elevation (Mohrig et al., 2000). As such, cells are considered superelevated when:

$$(\eta_{chan,low} - \eta_{adj,low}) \geq 0 \quad (9)$$

Our results are insensitive to values of  $\beta$  between 0.5 and 1. In addition to superelevation, an avulsion in our model must have a local gradient advantage over its previous pathway. We calculate this gradient over the first step of each flow path, as opposed to over the entire pathway (cf. Ratliff et al., 2018).



Avulsion triggering: Once a portion of a river is superelevated, some triggering event is necessary to initiate an avulsion. Predicting natural triggers is challenging because they can take the form of floods, ice damming, bank erosion, woody debris dams, neotectonics, meander bend cutoffs, beaver dams, bar migration, or other events that allow flow to escape normal channel confinement (Harwood and Brown, 1993; Smith et al., 1998; Ethridge et al., 1999; Jones and Schumm, 1999; Mohrig et al., 2000; Slingerland and Smith, 2004; Gibling et al., 2010, Morón et al., 2017). With that said, we know that trigger recurrence can only be as long as observed avulsion periods in natural river systems, which range from  $10^1$  years on the Kosi River megafan to  $10^3$  years on the Mississippi delta (Wells and Dorr, 1987; Aslan et al., 2005; Jerolmack and Mohrig, 2007). We set an average avulsion trigger period of 30 years by specifying a fixed probability of a trigger occurring on any given timestep. Since triggers cannot initiate avulsions in the absence of set-up via superelevation (Slingerland and Smith, 2004), this effectively sets a lower limit on avulsion period, but the actual period may be longer if there are no superelevated river segments along the active channel when a trigger occurs.

Avulsion pathfinding: Whenever an avulsion trigger occurs, avulsion pathfinding initiates from a randomly selected active channel cell that meets the set-up criteria. From here, the new channel path follows a steepness-weighted random walk if it remains in floodplain cells. Each step, the pathfinding avulsion can move into one of five cells (three downstream and two lateral). The cell is selected randomly, and the choices are weighted by steepness (see Table 1 for weighting scheme). Model outcomes are not sensitive over reasonable ranges of steepness weights, so long as all five directions are possible. The river is prevented from returning to its previous position and movement beyond the domain boundaries.

When a pathfinding avulsion is adjacent to an abandoned channel cell, the model checks to see if the abandoned channel cell is repulsive or attractive (Fig. 3C,D). Abandoned channel cells are repulsive when their levee heights above the adjacent floodplain ( $L_h$ ; meters) are larger than some multiple of the pathfinding avulsion flow depth ( $h_{avul}$ ; meters):

$$L_h > \alpha_R * h_{avul} \quad (10a)$$

$$L_h = (\eta_{aban,high} - \eta_{appr,low}) \quad (10b)$$

where  $\alpha_R$  is a nondimensional repulsion factor,  $h_{avul}$  is the threshold channel depth calculated with diffusion theory (Paola et al., 1992) assuming the flow is channelized during pathfinding, and  $\eta_{appr,low}$  is the low elevation in the adjacent cell from which the pathfinding avulsion channel approaches the abandoned channel.  $\alpha_R$  is a threshold for how tall levees must be to repulse advancing flow. Lower values are more repulsive since the threshold to repel is lower. A value of zero means that any positive value of  $L_h$  would cause repulsion.

Abandoned channel cells are attractive when  $h_{aban}$  (meters) is larger than some fraction ( $\alpha_A$ ) of mean flow depth:

$$h_{aban} > \alpha_A * \bar{h} \quad (11)$$

$\alpha_A$  is a threshold value describing how much remnant relief an abandoned channel must retain to capture flow. Lower values are more attractive since the threshold to attract is lower. If captured, the pathfinding avulsion will move in the direction of the lowest  $\eta_{aban,low}$ . This will continue unless there are no abandoned channel cells into which flow can proceed, which can



happen if the abandoned channel is discontinuous (Fig. 2), in which case the river is ejected back onto the floodplain and resumes steepness-weighted random walk.

325 Rivers that are repulsed or not captured by abandoned channels will proceed via steepness-weighted random walk until they exit the domain. If during pathfinding there are no viable moves, which can happen within floodplains bounded by abandoned channels that cannot be reoccupied (Fig. 2), the avulsion fails and all cells are reverted to their pre-avulsion state, and the model increments to the next timestep.

### 3.3.2 Floodplain processes:

330 Floodplain processes are applied to all abandoned channel and floodplain cells. These processes include rules for 1) overbank deposition; 2) subsidence; and 3) abandoned channel healing.

Floodplain deposition & subsidence: We implement a constant overbank deposition rate along grid rows that varies with distance from the mountain-front. There is no distance-from-channel-dependent component to overbank sedimentation (cf. Bridge and Leeder, 1979; Pizzuto, 1987), and instead the total floodplain aggradation for each row ( $A_{fp,tot}$ ; meters per year) is equal to the sum of a fixed rate ( $A_{fp,f}$ , meters per year) and a variable rate ( $A_{fp,v}$ , meters per year).  $A_{fp,v}$  linearly depends on the vertical distance between the highest elevation ( $\eta_{high,max}$ ) in that row and the elevation of a far-field floodplain cell that has never been visited by the active channel ( $\eta_{farfield}$ ). This vertical distance is normalized to units of mean channel depth. We assume that total overbank deposition on the floodplain ( $A_{fp,tot}$ ) cannot exceed subsidence so that the surface does not rise over time:

$$340 \quad A_{fp,tot} = \min \left\{ 0.5 * A_{fp,f} + 0.5 * A_{fp,v} * \frac{\eta_{high,max} - \eta_{farfield}}{\bar{h}} \right. \quad (12)$$

Equation (17) does not heal abandoned channels over time; healing is described in the following section. Finally, as a basic approximation of foreland basin style subsidence, we apply subsidence at each timestep at constant rates. These rates vary spatially via linear interpolation between a pair of rates representing proximal and distal values, with the proximal rates being two times greater.

345 Abandoned channel healing: Despite the critical importance that floodplain topography and abandoned channel healing timescales play in affecting channel network evolution in avulsing systems (Jerolmack and Paola, 2007; Reitz et al., 2010), there is no consistent choice of rules for implementing this phenomenon in models of avulsion. See the Discussion for a more comprehensive review of abandoned channel implementation in avulsion models. In our model, we implemented different abandoned channel healing styles to explore how they influence avulsion dynamics and landscape evolution. Within these styles, abandoned channels can be filled with sediment, have their levees eroded, or have both elevations adjusted toward the far-field floodplain (Fig. 4).

All healing modes adjust high, low, or both elevations linearly until a given endpoint is reached (Fig. 4). The healing rates are set to

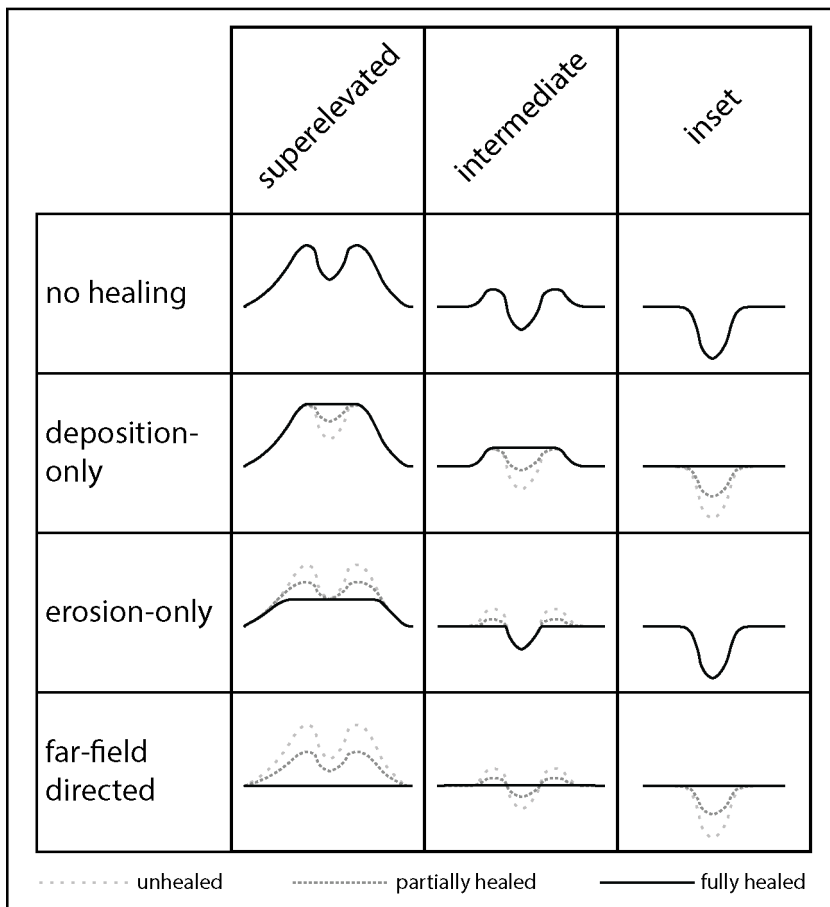


$$H_{high} = \alpha_{H,high} \frac{\bar{h}}{h_T} \quad (13a)$$

$$H_{low} = \alpha_{H,low} \frac{\bar{h}}{h_T} \quad (13b)$$

355

where  $\alpha_{H,high}$  and  $\alpha_{H,low}$  are the healing rate parameters and have values that range from -1 to 1, and  $h_T$  is the characteristic time needed to heal one mean channel depth, which we set as 55,000 years (see Discussion for details on this value). The first, deposition-only healing mode raises abandoned channel lows toward levee-tops, such that  $\alpha_{H,high} = 0$  and  $\alpha_{H,low} = 1$ . The second healing mode lowers levees toward channel-bases, such that  $\alpha_{H,high} = -1$  and  $\alpha_{H,low} = 0$ . The third healing mode  
 360 adjusts abandoned channel highs and lows toward the far-field floodplain elevation at rates of  $\alpha_{H,high} = -0.5$  and  $\alpha_{H,low} = -0.5$ . In all cases, once topographic highs and lows have achieved their final healing endpoints (Fig. 4),  $\alpha_{H,high}$  and  $\alpha_{H,low}$  rates are set to 0.



365

**Figure 4: Potential healing modes for different initial conditions of abandoned channels. Each healing mode has different endpoints depending on the initial channel emplacement: deposition-only adjusts each abandoned channel cell's low elevation toward its high elevation, erosion-only adjusts high elevations toward low elevations, and far-field directed adjusts both elevations towards the far-**





field floodplain elevation. As such, the deposition-only and erosion-only modes can result in topography that maintains positive topographic relief even once fully healed.

### 3.4. Experimental design

370 We ran four series of model experiments to investigate how abandoned channel attraction, repulsion, and healing influence avulsion dynamics. A summary of non-experimental and experimental parameters is provided in Table 3.

**Table 3: Model parameters used to generate figures**

Figure #	Run duration (Myr)	Avulsion trigger period (years)	Healing timescale ( $h_T$ , years)	Initialization length (meters)	Repulsion factor ( $\alpha_R$ )	Attraction factor ( $\alpha_A$ )	Healing mode
5	5	10	10,000	57,000	4.00	0.25	Far-field directed
6,8,9	1	30	55,000	122,500	4.00	0.25	Far-field directed
7	1	30	55,000	122,500	4.00	0.25	Variable (see Fig. 7)
10	5	30	55,000	122,500	Variable (see Fig. 11)	0.25	Far-field directed
11	5	30	55,000	122,500	4.00	Variable (see Fig. 12)	Far-field directed
12	10	30	55,000	122,500	4.00	0.25	Variable (see Fig. 13)

375 The first series consists of a single base run with  $\alpha_R = 4$ ,  $\alpha_A = 0.25$ , and far-field directed healing. Setting  $\alpha_R = 4$  means that flow is repulsed when levees are four times the height of the approaching flow; this allows some channels to be repulsive and others to not. Setting  $\alpha_A = 0.25$  allows channels to capture flow so long as they are deeper than  $\frac{1}{4}$  of a mean channel depth, consistent with flume experiments (Reitz et al., 2010) that show old, in-filling abandoned channels acting as attractors with little remnant relief. For abandoned channel healing, we employed far-field directed healing because its endpoint



of a totally flat plane is equivalent to that of diffusion on a laterally infinite plane, approximating the effects of floodplain  
380 diffusion without the computational cost.

Our second set of runs explored the importance of abandoned channel repulsion on where, when, and why avulsions occur by varying  $\alpha_R$  from -0.50 (most repulsive) to 8 (least repulsive), while holding  $\alpha_A = 0.25$ . Each run is a 5 Myr simulation using the far-field directed healing mode.

Next, a matching third set of runs was performed to investigate the effect of  $\alpha_A$  by varying it from 2.00 (least  
385 attractive) to 0 (most attractive) and setting  $\alpha_R = 4$ .

Our final set of runs investigated the role of abandoned channel healing mode without changing  $h_T$  (Fig. 4). We hold  $\alpha_A$  and  $\alpha_R$  constant over each 10 Myr run.

### 3.5 Analysis

We analyzed the planform appearance of generated topography and the location of avulsions for each run. For figures  
390 showing planform appearance (Fig. 5; Fig. 6; Fig. 10-12), we normalized each cell's high elevation relative to the  $\eta_{farfield}$  for its row. We did this because megafans are low-relief features, and the change in elevation along dip otherwise overwhelms the signal (Fig. 5). We quantified avulsion locations by recording the straight-line distance from the mountain-front to each avulsion. These data were binned every 6.25 km and plotted as histograms showing the number of avulsions moving away from the upstream boundary. These values are normalized to the bin with the greatest occurrence. For Fig. 6, we measured and  
395 binned avulsion locations in the same way for a second run without relative superelevation, but normalized this histogram to that of the base run to display the overall reduced number of avulsions. We also analysed avulsion locations by creating smoothed (50 kyr moving window average) curves of recorded distance to the mountain-front that show how median and 95<sup>th</sup> percentile (i.e., distal) avulsion locations change over the course of simulations. Finally, we analyzed differences between the proximal and distal domains for our base run by tracking the along-strike position of the active channel at two distances (12.5,  
400 50 km) from the mountain-front for every timestep (Fig. 7).

## 4. Model results

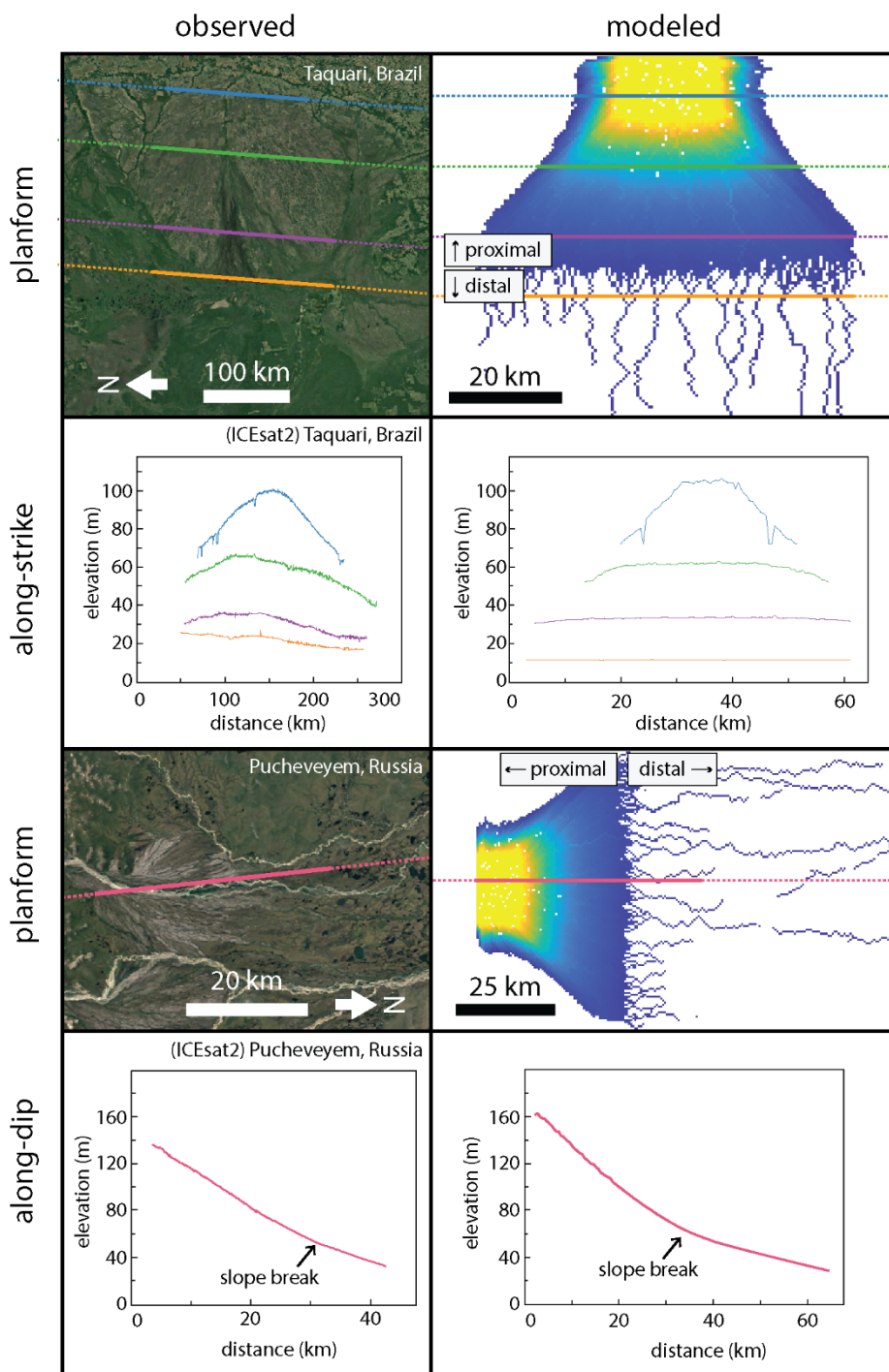
### 4.1. Base run and validation

We validated our model results by comparing model output for our base run with megafan topography from ICESat-2 (Neuenschwander et al., 2020) via the OpenAltimetry platform (Khalsa et al., 2020). ICESat-2 is a continuously measuring  
405 (10 kHz, ~0.7 m between points on the ground) satellite that collects vegetation-penetrating laser altimetry (Neuenschwander and Pitts, 2020). ICESat-2 offers greater precision than radar-derived elevation at the cost of limiting data collection to ~north-south oriented linear tracks. Our model recreates the change in along-strike profiles of the Taquari megafan, showing broad, low-relief convex-up topographic profiles proximally that transition to nearly flat profiles in the distal domain (Fig. 5). Along-



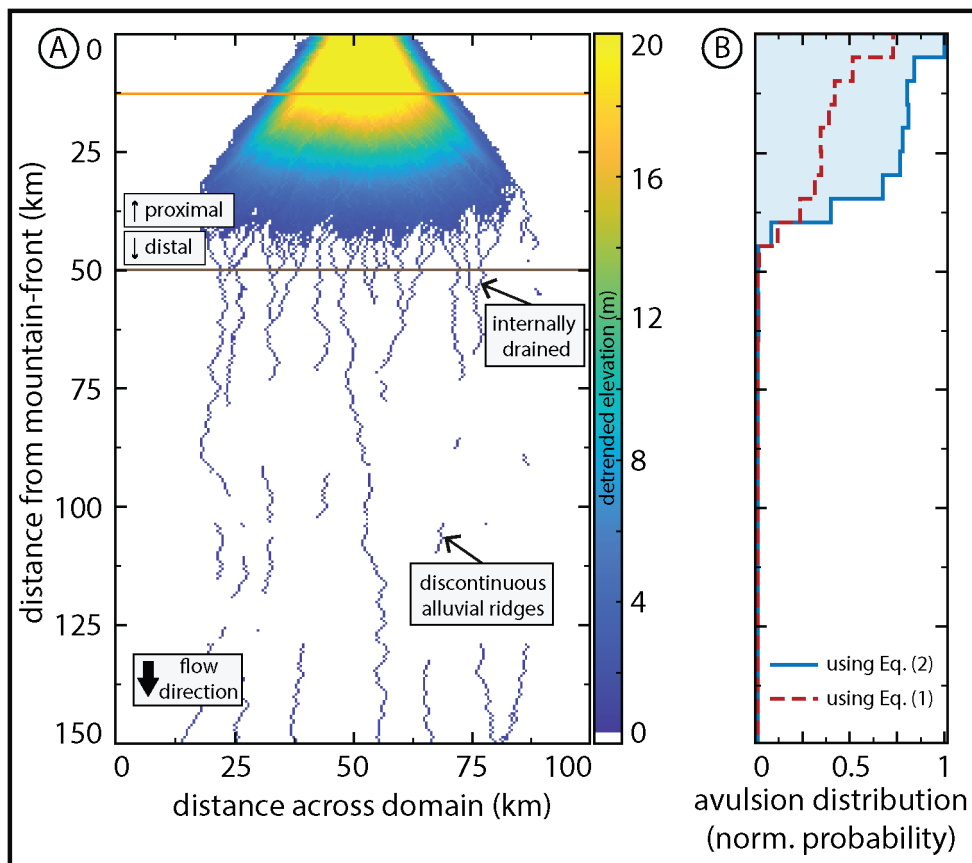
dip comparisons on the Pucheveyem fan (Fig. 5) are also favorable, showing similar low-relief slopes ( $\theta:10^{-3}$ ). These slopes  
410 change abruptly at a topographic break marking the end of the fan topography, with a shallower gradient in the distal domain.

The model produces two distinct domains, consistent with earlier remote sensing observations (Fig. 1). The proximal  
domain is a zone of sediment distribution created by repeated avulsions; it has a steeper slope (Fig. 5) and the abandoned  
channels that create the topography are radially distributive (Fig. 6A). In this domain, frequent channel avulsion causes small  
lateral adjustments to river position, filling topographic lows (Fig. 7A). Avulsion probability is highest at the apex because  
415 that is where sediment is introduced (Fig. 6B). In contrast, the distal domain is a zone with a dominantly tributive geometry;  
it has a shallower slope (Fig. 5) and is much more sparsely channelized (Fig. 6A). In this domain, the active channel switches  
between fewer, more-persistent channels (Fig. 6A; Fig. 7A). Flow becomes confined to these more-persistent channels because  
avulsions that occur upstream are quickly captured and routed into one of a finite number of pre-existing pathways (Fig. 7A).  
Distal abandoned channels that are occupied infrequently can partially or fully heal between revisitations, creating  
420 discontinuous alluvial ridges (Fig. 2; Fig. 6). Avulsion probability rapidly decreases past the fan boundary (Fig. 6B). Past the  
fan boundary, along-strike topographic profiles become nearly flat (Fig. 5), and this compares favorably to previous  
observations of megafans (Hartley et al., 2010a; Bernal et al., 2011).

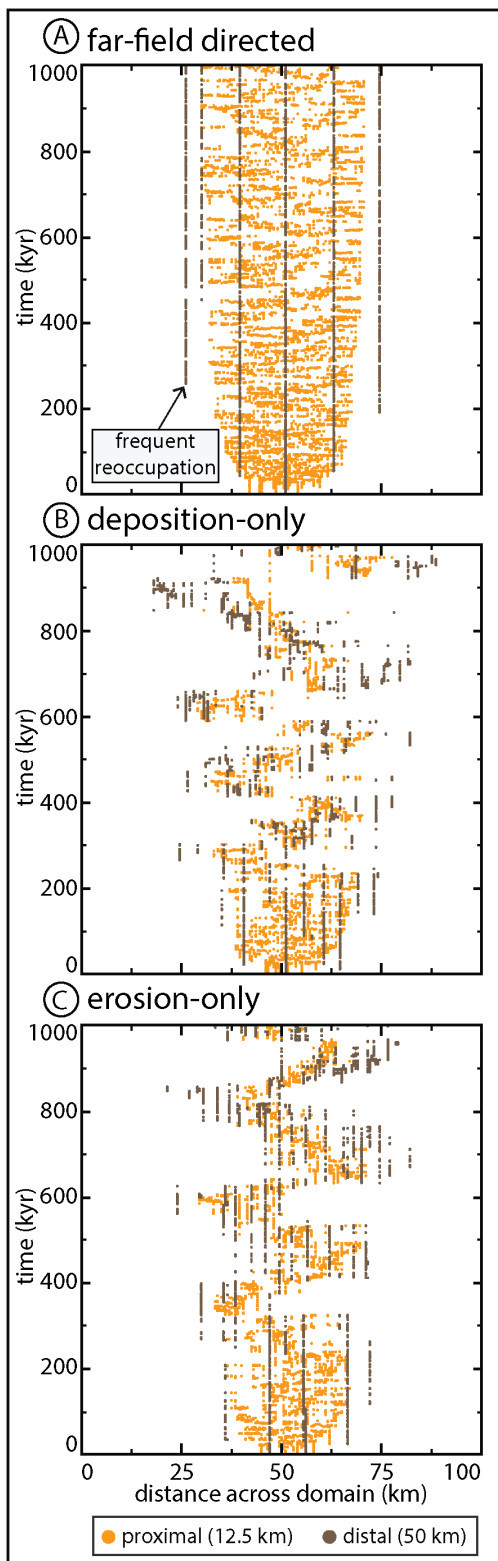


425 **Figure 5: Megafan topography from model output compares favorably with real megafans observed in both the along-strike and along-dip profiles direction. Note the exceptional vertical exaggeration in the Taquari along-strike profiles. satellite images are USGS/NASA Landsat/Copernicus, © Google Earth.**





430 **Figure 6:** (a) Planform output of detrended high elevations from the base run. Location of active channel not shown. The model produces two distinct domains (proximal and distal) in addition to several marked features which compare well with observed megafans in the real world (Fig. 1). Orange and dark brown horizontal lines show the proximal and distal measurement locations, respectively, for Fig. 7. (b) A histogram (bin-width 6.25 km) showing the downstream distribution of avulsion loci. Blue line corresponds to output in (A), whereas the dashed red line is the same as (a), but requires one full channel depth of aggradation to achieve super-elevation (Eq. (1)) instead of measuring elevation relative to adjacent cells (Eq. (2)). Vertical axis scale for (b) is the same as (a).





440

**Figure 7: Active channel position histories over 1 Myr at two distances from the mountain-front for three runs. In each run, only one channel position is possible per timestep. (a) A run using the same parameters as Fig. 6. Note frequent and continued reoccupation for distal river positions. (b) and (c) show runs identical to (a) except the healing modes are deposition-only and erosion-only, respectively (Fig. 12A). These runs show similar behavior to (a) in early years but transition to lobe-switching behavior. Distances to the mountain-front are illustrated via horizontal bars in Fig. 6A.**

#### 4.2 How abandoned channels affect avulsion dynamics

Abandoned channels affect the timing and location of avulsions in four different ways: 1) superelevation shortcutting, 2) inheritance, 3) post-avulsion diffusion of the channel-bed, and 4) confluence aggradation. Each is discussed below.

We implemented avulsion set-up by measuring superelevation of an active channel relative to surrounding floodplain topography (Eq. (2); Fig. 3). To investigate the effect of abandoned channels on this set-up, we performed an additional run that is equivalent to our base run in Fig. 6 except for requiring each cell to aggrade a specified fraction of a channel depth between each avulsion (Eq. (1); Fig. 6B). Compared to this run, the base run had a greater number of avulsions, especially on the megafan surface downstream of the apex (Fig. 6B). Measuring superelevation relative to floodplains allows local topographic lows associated with former abandoned channels to provide attractive locations for avulsion initiation, shortcutting superelevation timescales (Jerolmack and Mohrig, 2007). Therefore, a densely channelized proximal domain generates additional superelevation opportunities, spatially concentrating avulsions (Fig. 6B).

Abandoned channels also affect avulsion set-up indirectly through reoccupation mechanics. Superelevation is inherited when avulsive flows reoccupy former abandoned channels. In a superelevated channel reach, an avulsion will strand superelevated portions of the river that are downstream of the avulsion locus (discontinuous alluvial ridges in Fig. 6A). In this way, avulsions can leave behind abandoned channels that may require minimal aggradation to achieve superelevation if they are reoccupied before being healed, particularly if those channels are themselves adjacent to abandoned channel topography that provides relative superelevation.

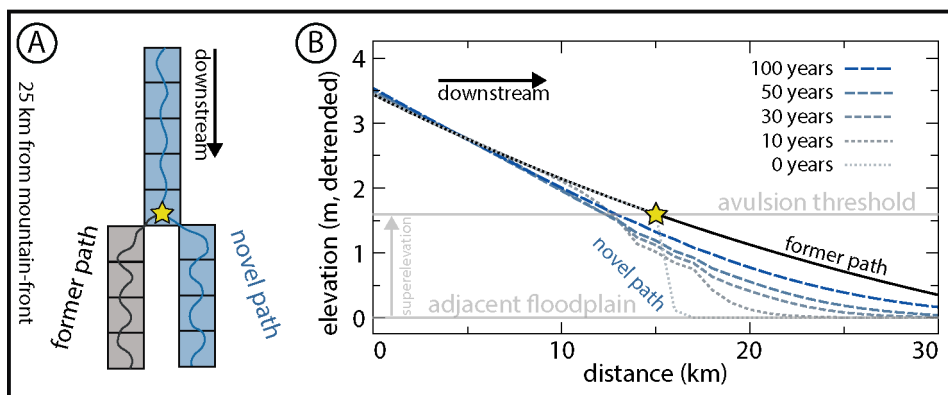


**Figure 8: Model example showing channel evolution immediately after an avulsion. (a) Planform arrangement of the parent channel and avulsion node, with both pathways of equal length. (b) Detrended elevation of the parent channel (relative to the adjacent floodplain) and new avulsion pathway upstream and downstream of the avulsion node. Immediately prior to the avulsion (black line), all cells upstream of the avulsion node are superelevated and are equally likely to avulse if a trigger occurs. After the avulsion, gradual knickpoint propagation upstream reduces superelevation. Downstream of the avulsion site, there is significant deposition that reduces the time to superelevation.**

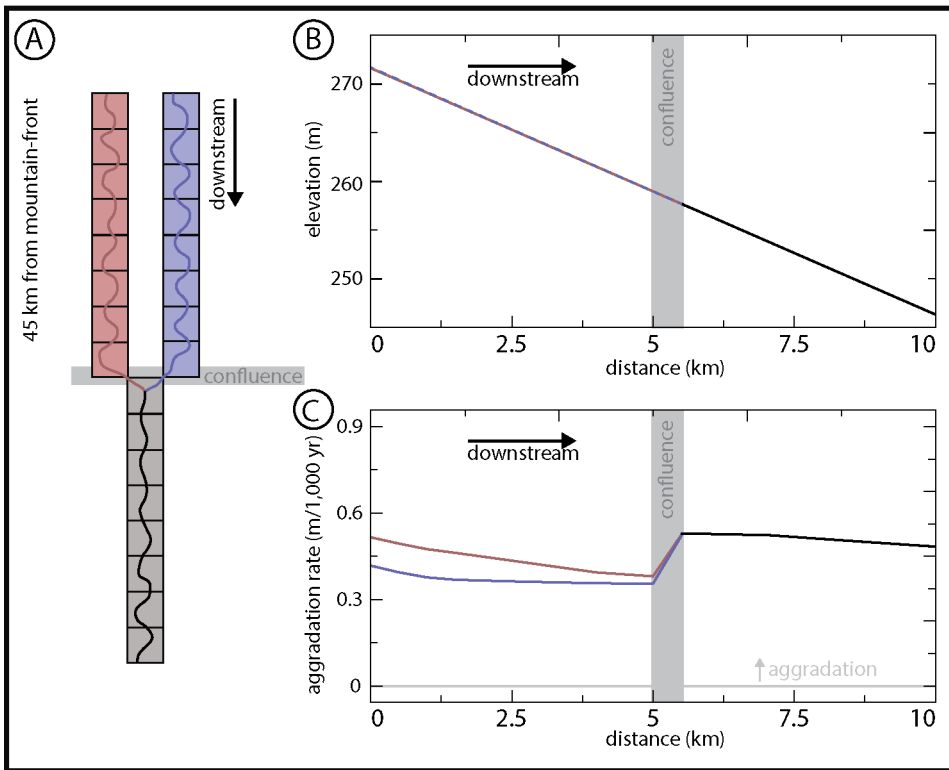
460



465 In our model, avulsion set-up is also affected by local effects immediately after avulsions due to transient diffusion.  
This occurs in two ways. Firstly, superelevated cells upstream of the avulsion locus are not instantly lowered but instead require  
time for the knickpoint to propagate upstream (Fig. 8). In our simulation, the post-avulsion upstream reduction in channel bed  
superelevation proceeded gradually, migrating only several kilometers 100 years after an avulsion (Fig. 8). In this way, an  
avulsion does not instantly undo the avulsion set-up of cells upstream and future triggers can still cause avulsions to occur  
470 over this domain. Secondly, immediately downstream of an avulsion locus there is significant aggradation; a channel can  
diffuse nearly a meter of sediment into a downstream active channel cell within a decade (Fig. 8). In the case that these  
downstream cells are themselves already nearly superelevated, this can provide sufficient aggradation above the adjacent  
floodplain to set-up these cells. This effect is even more pronounced when new active channel cells are adjacent to abandoned  
channel lows, and thus have lower superelevation thresholds.

475 In our model, we observed abandoned channel confluences wherever a pathfinding flow is captured by a previous  
abandoned channel. Captured channels follow steepest-descent pathfinding within the network of occupiable abandoned  
channel cells. Within the distal, tributive domain, the number of possible abandoned channel pathways that can be occupied  
decreases with increasing distance from the mountain-front (Fig. 6A; Fig. 7A). This allows locations downstream of  
confluences to be more continuously occupied while the flow switches pathways upstream. This has important effects on  
480 avulsion because more aggradation occurs downstream of the tributary junction. Consider a scenario where avulsions on the  
fan always route flow into one of two possible paths (Fig. 9A,B). The pathway downstream of the confluence is occupied  
100% of the time while each parent pathway is occupied approximately half of the time. As channel-bed aggradation occurs  
only during active channel occupation, aggradation downstream of the confluence can therefore be greater than that observed  
in either upstream pathway (Fig. 9C). As such, in the distal domain, abandoned channel reoccupation should preferentially  
485 focus avulsions downstream of abandoned channel confluences.





490 **Figure 9: Model experiment showing channel evolution at an abandoned channel confluence. (a) Planform arrangement where the channel avulses between the red and blue pathways whenever normal avulsion criteria are satisfied. (b) Elevations of the red, blue, and gray channel segments upstream and downstream of the confluence. These elevations are not detrended. The blue channel profile is dashed to not obscure the red channel profile. (c) Aggradation rates over a 3,000 year period along the three channel segments. Repeated avulsions mean that the red and blue channels alternate deposition, while the gray channel downstream is constantly occupied leading to a faster aggradation downstream of the confluence.**

### 4.3 Abandoned channel repulsion

We observed the effects of varying  $\alpha_R$  on both planform appearance and the location of avulsions with a constant  $\alpha_A$   
 495 (Fig. 10). Increasing repulsion (decreasing  $\alpha_R$ ) extends the proximal domain farther downstream; increasingly repulsive runs are increasingly distributive, generating fewer tributary confluences (Fig. 10A). Further, runs that are highly repulsive do not generate the abrupt downstream change in avulsion frequency seen when  $\alpha_R > 2$ . Instead, highly repulsive runs show relative avulsion frequencies that follow a power-law-like distribution with distance from the mountain-front (Fig. 10A).

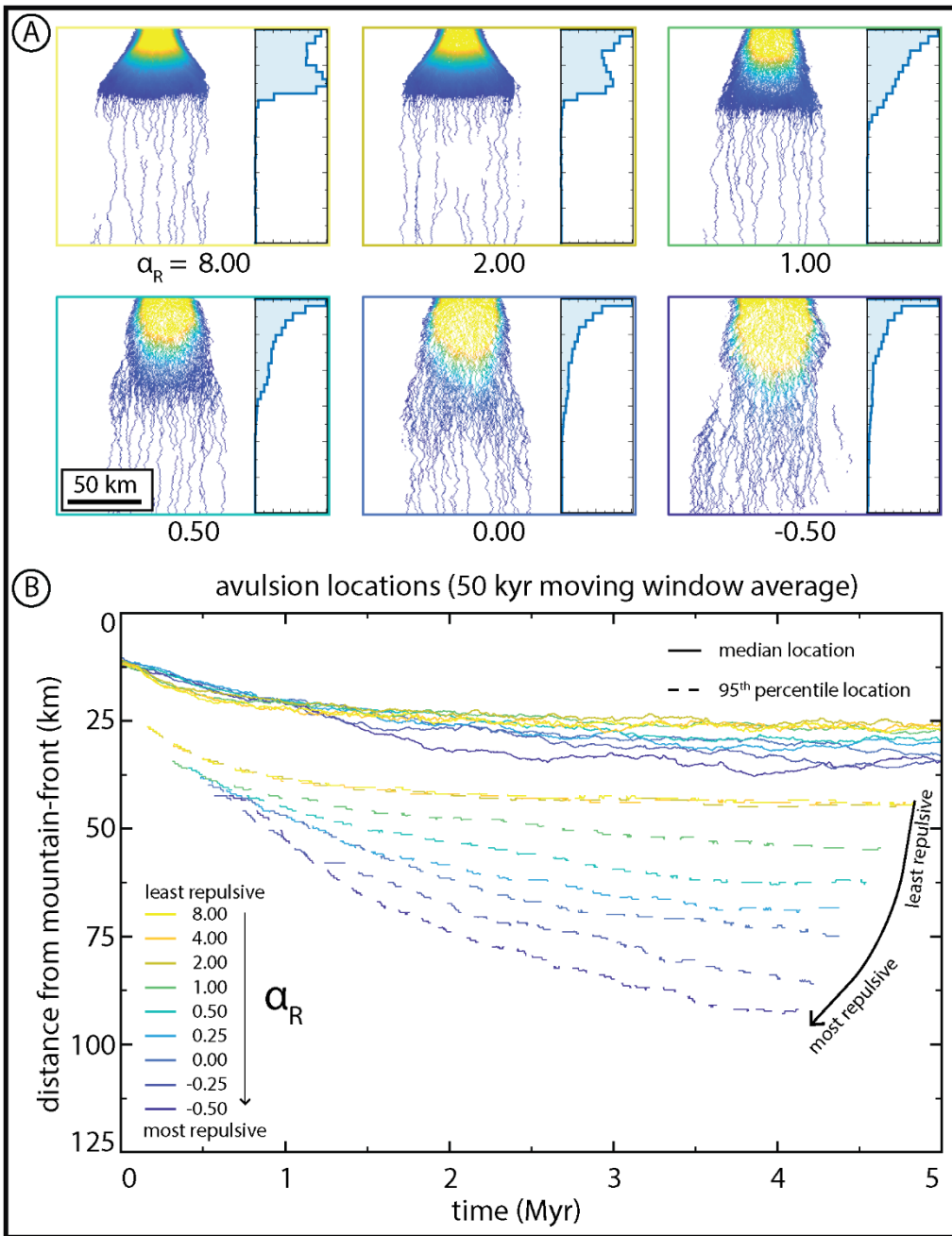
The proximal domain propagates farther downstream when  $\alpha_R$  is smaller (more repulsive) because avulsion location  
 500 propagates farther downstream (Fig. 10B). While all avulsion location curves show a downstream progradation of avulsion locations during runs as the fan grows, both the median and 95<sup>th</sup> percentile shift downstream between runs with decreasing  $\alpha_R$ . Median avulsion locations are less affected than 95<sup>th</sup> percentile curves, indicating that distribution skewness increases. The greatest shift in avulsion locations occurs between simulations employing  $\alpha_R \leq 1.00$  (i.e., where avulsive flows must be equal to or greater than levee heights above surrounding floodplains to reoccupy).



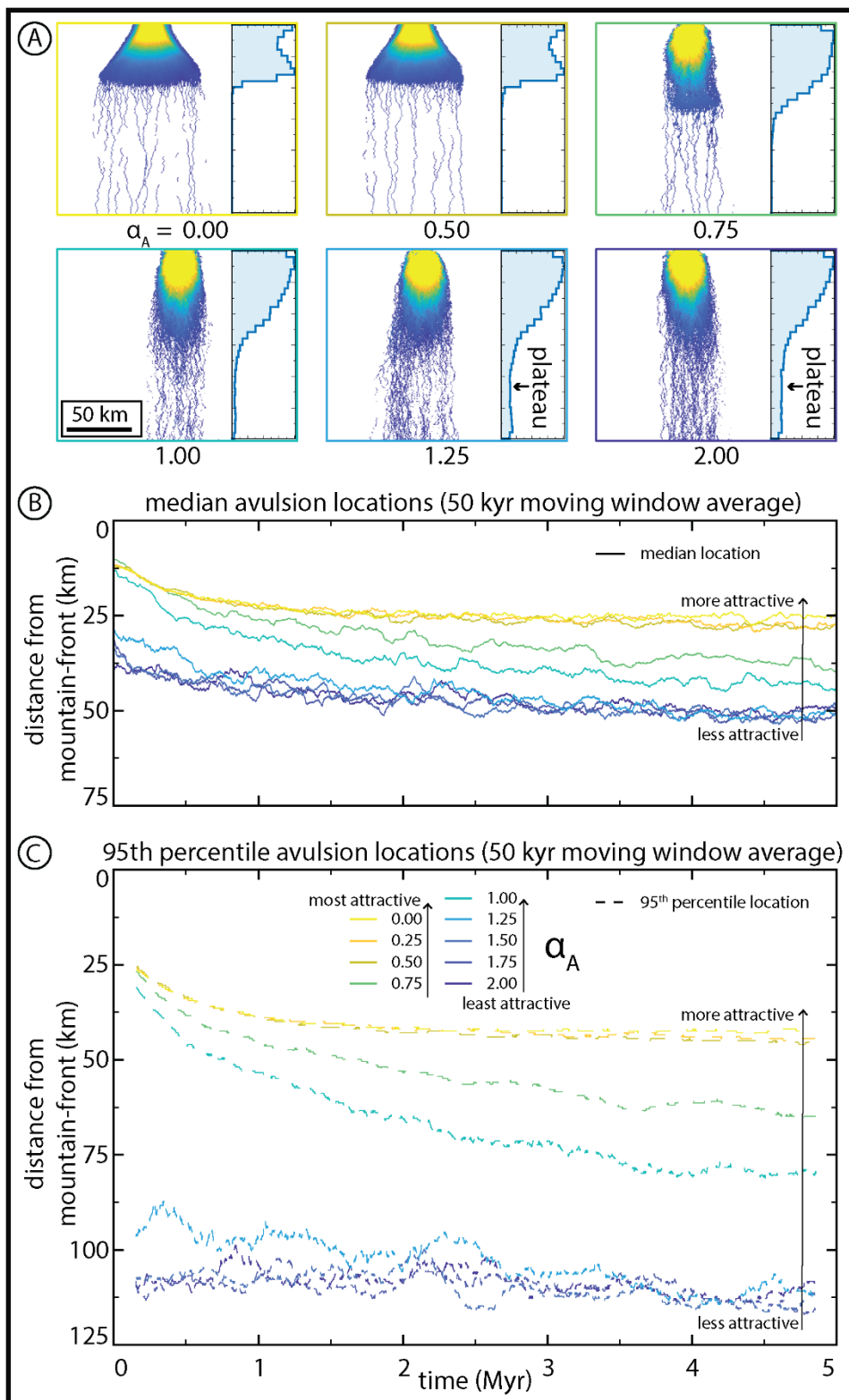
505           Increasing repulsiveness (decreasing  $\alpha_R$ ) pushes avulsions farther from the mountain-front because flow in the proximal domain is concentrated into fewer channels, allowing for sediment (and therefore superelevation) to propagate farther downstream (Fig. 10). As a contributing effect, runs with lower  $\alpha_R$  create more internally drained basins that themselves cause avulsions to fail. Since failed avulsions cause the timestep to increment without changing river positions, the time between successful avulsions is greater in runs with many failed avulsions, and sediment can thus propagate farther along active  
510 channels. This encourages channels in the distal part of the model to superelevate and avulse more often.

#### 4.4 Abandoned channel attraction

Abandoned channel attraction dynamics also impact both avulsion locations and planform appearance during model runs (Fig. 11). With a constant  $\alpha_R$  and increasing abandoned channel attraction (decreasing  $\alpha_A$ ), the transition from distributive to tributive domains shifts up-domain and fan width increases (Fig. 11A). When  $\alpha_A$  is large (low attractiveness), model output  
515 resembles a series of weighted random walks because abandoned channels rarely capture flow and steepness weighted random walk determines channel position. Like the repulsion simulations, both the median and 95<sup>th</sup> percentile avulsion locations are affected by changing attraction parameters (Fig. 11B). Decreasing  $\alpha_A$  (increasing attractiveness) pulls avulsions towards the mountain-front, and the greatest change is for  $\alpha_A$  between  $\sim 0.50$  and  $1.50$ . Minimal change occurs for  $\alpha_A$  values above and below this range. In contrast, when  $\alpha_A$  increases (attractiveness decreases), the fan lengthens and avulsions occur farther down-  
520 domain because fan surfaces host abundant abandoned channels that influence avulsion dynamics. This interpretation is supported by the avulsion histograms, where low-attractiveness runs show a non-zero avulsion frequency plateau in the distal reaches and a more gradual downstream reduction in frequency than in more-attractive runs (Fig. 11A).



525 **Figure 10: The effect of abandoned channel repulsion on (a) planform appearances and normalized avulsion location histograms, and (b) characteristic avulsion locations through time. Decreasing  $\alpha_R$  causes avulsion location to move downstream. These changes are more pronounced for 95<sup>th</sup> percentile locations. Color scale for inset planform appearances is the same as in Fig. 6.**





530 **Figure 11: The effect of abandoned channel attraction on (a) planform appearances and normalized avulsion location histograms, and (b,c) characteristic avulsion locations through time.  $\alpha_A$  legend and x-axis scale in (c) applies to (b) as well. Note the difference in y-axis extents between (b) and (c). Between  $\alpha_A$  values of 0.50 and 1.50, increasing  $\alpha_A$  causes predictable increases in the distance between the mountain-front and median and 95<sup>th</sup> percentile avulsion locations. These changes are more pronounced for 95<sup>th</sup> percentile locations, indicating greater skewness. Color scale for inset planform appearances is the same as in Fig. 6.**

#### 4.5 Healing mode

The healing mode determines how abandoned channels are gradually removed from the floodplain. By conducting  
535 10 Myr base runs with different healing modes, we found that the deposition-only and erosion-only runs generated fans that nearly entirely filled up the simulation space over the course of several million years (Fig. 12). This occurs because the remnant topography of abandoned channels was never entirely removed by healing between visitations. This is true even for the erosion-only run as, by definition, channels that achieve superelevation before abandonment have bases that are higher than surrounding floodplains. Since healing in erosion-only runs terminates once levees reach channel-beds, superelevated  
540 abandoned channel-beds on the floodplain remain indefinitely.

Healing mode affects avulsion location and introduces a new dynamic for fan growth. In erosion-only runs, the avulsion location progrades the farthest into the basin (Fig. 12B). Interestingly, the median and 95<sup>th</sup> percentile time series for deposition-only and erosion-only avulsion locations show spikes that represent avulsion location rapidly moving toward the mountain-front. These spikes represent lobe switching events, where avulsion loci shifted proximally as depositional space  
545 lower on the fan is filled and apical avulsions reroute flow to new regions on the fan surface (Fig. 7B,C; Supplemental Videos 1-3; DOI: 10.5446/54887). This compares well to observations of real-world megafans where deposition is interpreted to have occurred on discrete lobes (Chakraborty et al., 2010; Zani et al., 2012; Assine et al., 2014; Weissmann et al., 2015; Pupim et al., 2017). Lobe switching emerges in the model when deposition in a particular region causes a lobate area to become raised relative to other areas on the floodplain. This limits the accommodation available over this area, leading to a slope disadvantage  
550 over other regions on the floodplain. Future apical avulsions can redirect flow to these other lower regions, which will themselves eventually become raised and begin the cycle anew. Lobe switching does not occur during the earliest stages of fan growth because there is ample accommodation on all faces of the fan.

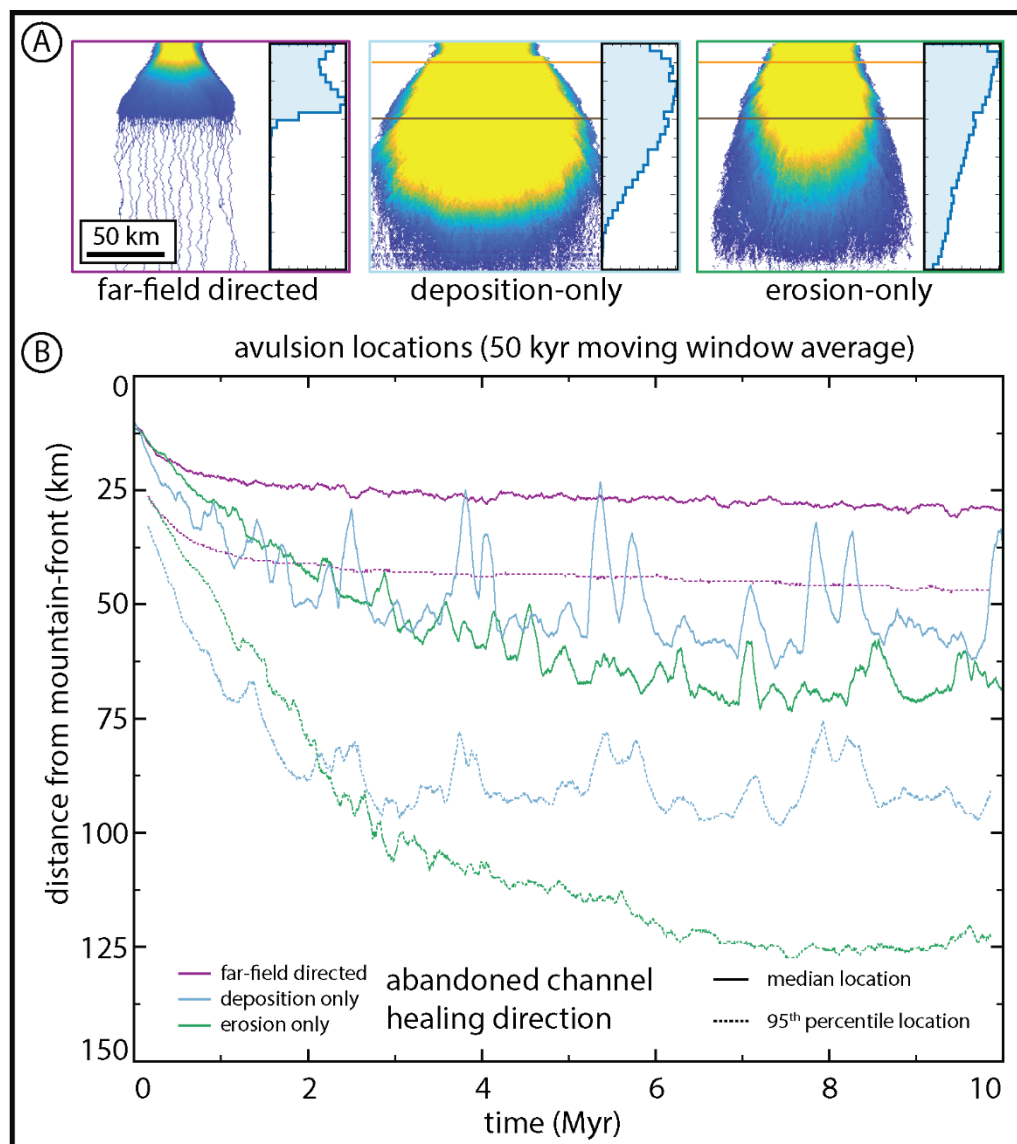
In contrast to the deposition-only and erosion-only runs, the far-field directed simulation achieved dynamic equilibrium relatively quickly and maintained a well-defined boundary between the proximal and distal domains for the  
555 remainder of the run. This occurs because it is the only healing mode that completely removes abandoned channel topography from floodplains. As such, this is the only healing mode that erases the topographic, attractive, and repulsive “memories” (*sensu* Reitz et al., 2010) of abandoned channels. Lobe switching on the same timescale is not observed in these runs because, unlike the deposition-only and erosion-only runs, far-field directed runs do not preserve topography indefinitely and alluvium is removed sufficiently quickly to provide accommodation on all faces of the fan throughout the run.

560 It is important to note that both the erosion-only and deposition-only runs exhibited the typical separation of planform space into two domains as they prograded, until the proximal domain encountered the edge of simulation space and the only





565 12A).



570 **Figure 12: The effect of healing mode (a) planform appearances and normalized avulsion location histograms, and (b) characteristic avulsion locations through time. Runs are identical other than employing different abandoned channel healing modes. Orange and dark brown horizontal lines show proximal and distal (respectively) distances from mountain-fronts for Fig. 7B (deposition-only) and 7C (erosion-only). Color scale for inset planform appearances is the same as in Fig. 6.**



## 5. Discussion

### 5.1 Abandoned channels in avulsion models

Our model was designed to investigate the role of abandoned channels as both topographic repulsors and attractors during avulsion pathfinding. In doing so, we demonstrated effects on avulsion location and planform landscape evolution. We showed that abandoned channels affect the frequency and position of avulsions. Importantly, we demonstrated that the typical low-relief megafan with a transition from proximal (distributive, densely channelized) to distal (tributive, sparsely channelized) domains originates only when avulsion repulsion is infrequent and attraction is frequent (Fig. 10; Fig. 11). As such, when creating avulsion models, it is worth explicitly addressing abandoned channel creation, rate of healing, mode of healing, and interactions with future avulsion set-up and pathfinding because these factors fundamentally change avulsion dynamics and planform appearance of fluvial systems.

Abandoned channels and their impact on avulsion are usually ignored or grossly simplified in simulation models, especially in alluvial architecture models that simulate a 2D cross-section. The pioneering Leeder (1978), Allen (1978), and Bridge and Leeder (1979) models connected avulsions to alluvial architecture by creating 2D vertical slices of stratigraphy that result from channel avulsion across a basin over time. These models required heuristic rules about where successive rivers would be emplaced, including choosing locations randomly (Leeder, 1977), according to lowest elevation, (Bridge and Leeder, 1979), or randomly with abandoned channel repulsion (Allen, 1978). While their resulting stratigraphic sections were fairly insensitive to these differences (Hajek and Wolinsky, 2012), modern successors of these cross-section alluvial architecture models (e.g., Chamberlin and Hajek, 2015, 2019) have demonstrated that choosing different avulsion emplacement rules exerts a significant control on resulting stratigraphy. These rules position future channels along random (along a uniform distribution), compensational (at the lowest topographic elevation), or clustered (likelier to be nearer to the previous channel position) distributions. While these rules prescribe the cross-basin location of successive channels without needing to resolve planform pathfinding, it is unclear how abandoned channels affect or reflect each rule.

Our results provide mechanistic insight into the floodplain conditions that lead to different avulsion channel placement rules. An interesting outcome of our model is that the position of successive channels after avulsion follows different rules in proximal and distal domains (Fig. 7). In the proximal domain, avulsion pathways follow steepest-descent pathfinding that should generate compensational stratigraphy by seeking local, not global, topographic lows (Fig. 7). This correlates to a scheme where an avulsion is placed at the lowest elevation within a permissible lateral range (e.g., wide- or narrow-zone clustering of Chamberlin and Hajek, 2015), and compares well to limited observational data showing that most avulsions initiate into topographic lows and travel relatively small lateral distances before joining abandoned channels (Edmonds et al., 2016; Valenza et al., 2020). In our deposition-only and erosion-only runs, emergent lobe switching provides an additional scale of clustering that can control channel positions (Fig. 7; Fig. 12). In the distal domain, however, flow routing instead switches between a small number of active channels in a network, each of which can heal if they are not revisited for a sufficient amount of time (Fig. 7). This compares better to the experimental model and flume observations of Jerolmack and Paola (2007)



and Reitz et al. (2010). Finally, in the low-attractiveness cases ( $\alpha_A \geq 1$ ; Fig. 12), new channel pathways are determined entirely  
605 by slope-weighted random walk, which would compare closest to the compensational avulsion placement schemes of  
Chamberlin and Hajek (2015) or Bridge and Leeder (1979). As a caveat, when abandoned channels influence pathfinding, our  
model shows that it is not always possible for avulsions to find the globally lowest point in the whole domain for a given cross-  
section (cf. Bridge and Leeder, 1979) because there may be high topography in-between that prevents pathfinding. This is  
particularly evident in the lobe switching shown in Fig. 7B and Fig. 7C, where the global lowest point may exist outside of  
610 lobe deposition, but no viable route exists to reach that point.

To avoid making explicit assumptions about channel emplacement, a parallel lineage of avulsion models resolve  
avulsion dynamics and pathfinding in a planform basin. As such, these avulsion models require rules for hydrodynamics,  
sediment transport, and avulsion set-up, initiation, pathfinding, and stabilization, but allow for a more sophisticated interaction  
between avulsion pathfinding and floodplain topography (including abandoned channels) than can be resolved in cross-section  
615 models (Hajek and Wolinsky, 2012). Whenever these models incorporate steepness (with or without random noise) into  
avulsion pathfinding, and do not instantly erase the topographic alterations made by abandoned channels on landscapes,  
pathfinding is implicitly controlled by abandoned channels (e.g., Mackey and Bridge, 1995; Coulthard et al., 2002; Sun et al.,  
2002; Jerolmack and Paola, 2007; Reitz et al., 2010). As a broad classification, there are at least four assumptions that can  
describe the fate of these abandoned channels: i) avulsed channels do not leave behind abandoned channels on floodplains  
620 (instant healing; Ratliff et al., 2018, 2021), ii) abandoned channels do not change after avulsion (no healing), iii) abandoned  
channels are instantly healed after some fixed number of timesteps (Reitz et al., 2010), or iv) abandoned channels are healed  
gradually over time by adjusting their channel-base and/or levee-top elevations (Jerolmack and Paola, 2007). The first three  
assumptions do not allow abandoned channel to act as both repulsors and attractors, which is inconsistent with observations  
of avulsing rivers (Edmonds et al., 2016; Valenza et al., 2020). Further, the first assumption generates no abandoned channel  
625 topography on floodplains, which is inconsistent with our observations (Fig. 2).

## 5.2 Floodplain topography and evolution

Our model shows that lobe switching on megafans only appears under certain abandoned channel healing rules (Fig.  
7; Fig. 12). Floodplain topography, including abandoned channels, is thus a critical control on avulsion dynamics and landscape  
evolution and modelers who wish to recreate foreland basin topography must be conscious of how they choose to implement  
630 abandoned channel healing. This result emphasizes Jerolmack and Paola (2007)'s identification of the remarkable lack of  
knowledge regarding the competing processes of topographic construction and destruction on floodplains. The principal  
topographic features of floodplains in aggradational (*sensu* Weissmann et al., 2015) settings appears to be abandoned channels,  
including both topographic highs and lows (Fig. 2). Understanding the extent to which abandoned channels and floodplain  
topography control avulsion dynamics in natural systems, requires a better understanding of floodplain topography. While  
635 little is known about the constructive and destructive processes in action on floodplains, we can speculate on the evolution of  
abandoned channels using observations from both degradational and aggradational settings (Hartley et al., 2010b).



There is field evidence that abandoned channels heal. During floods, overbank sediments can preferentially deposit in abandoned channel topographic lows (Wolman and Eiler, 1958; Schumde, 1963; Bridge and Leeder, 1979; Lewis and Lewin, 1983; Farrell, 1987; Nanson and Croke, 1992; Tooth et al., 2002; Jerolmack and Paola, 2007). This healing, however, can be undone in some cases by scouring from future flooding events (Wolman and Leopold, 1957; Wolman and Eiler, 1958; Schumde, 1963; Bridge and Leeder, 1979). What happens to abandoned channel highs, on the other hand, is not well understood. High elevation on floodplains could conceivably be eroded during subsequent flood events, or gradually diffused, similar to hillslopes (Roering et al., 1999). While floodplain slopes are characteristically low, biologic disturbance is high; it is not clear whether diffusion should also describe the evolution of alluvial floodplain topographic highs. Complicating matters, sediment deposition during overbank flows has also been observed atop flat or even positive floodplain topography, promoting self-sustaining topography that also hinders abandoned channel healing (Jahns, 1947; Wolman and Eiler, 1958; Schumde, 1963; Nanson, 1980).

Given the extent of these unknowns, considerable insight about floodplain evolution could be gained from highly detailed investigations of channel levees and beds before and after avulsions. The relative degree of abandoned channel attraction and repulsion, and thus the appropriateness of our parameters  $\alpha_R$  and  $\alpha_A$ . Longitudinal studies of this nature could also understand the rate at which abandoned channels are healed (and thus no longer affect pathfinding) and the direction or mode in which they are healed, which we found to have important implications on avulsion dynamics (including lobe switching) and long-term planform morphology (Fig. 12). It may be that healing proceeds in different directions and at different rates in different settings in the basin, which will have important impacts on the spatial variation of avulsion dynamics and planform morphologies. We note that detailed work on the time-fate of topographic highs associated with abandoned channels is especially lacking in the body of literature.

### 5.3 Next steps & predictions for comparison with field sites

We make several predictions that can motivate future observational and field studies. To begin, one key prediction is that in the proximal portions of foreland basins, avulsions should be most-frequent on the surfaces of megafans (e.g., Fig. 6B). These results compare favorably to the limited data available (Valenza et al., 2020) and can be tested by future observations of avulsions in the available and future remote sensing record. The emergence of future datasets on real-world avulsions should be able to confirm or deny the predicted abrupt, non-linear change in relative avulsion frequency with increasing distance from mountain-fronts on megafans (Fig. 6B). These data about the location of avulsions should also allow testing of other predictions from our model, including that avulsion in the distal domain of aggradational settings is more common immediately downstream of abandoned channel confluences due to a greater total occupancy duration and therefore greater total aggradation than either parent pathway immediately upstream (Fig. 8).



## 6. Conclusion

Abandoned channels are pervasive on megafans in modern foreland basin settings. These locations also have some of the highest avulsion rates in the observational record, and thus necessitate considering the role of abandoned channels on avulsion dynamics and planform evolution in modeling efforts. We developed and presented a model that tests the interaction between abandoned channels and an avulsing river. Our model intrinsically generates two distinct domains, proximal and distal, in good comparison with remote sensing and previous research. We demonstrated that abandoned channels may shortcut avulsion superelevation timescales in these settings by providing topographic lows adjacent to potential avulsion loci, by providing remnant superelevation that can be inherited by future captured avulsions, including downstream of abandoned channel confluences, and by transient knickpoint propagation that allows superelevated rivers to remain superelevated upstream of the initial avulsion. The upshot of these factors is that avulsions are proportionately much more common over the proximal distributive domain compared to the distal tributive one. We showed that tuning the degree to which abandoned channel repulsion and attraction occur in simulations causes predictable changes in avulsion location during those runs, whereby increasing repulsion pushes avulsions farther from the mountain-front, and increasing attraction ‘pulls’ them closer. Next, we demonstrated the important role that abandoned channel healing mode has on gross planform morphology, particularly over deep time, and that the proximal domain should grow until filling all available space in systems that heal via deposition-only or erosion-only. Finally, we have highlighted opportunities for future work by field workers and remote sensors in understanding the role that floodplain topography plays on avulsion dynamics, and the fate of floodplain abandoned channel topography.

## 7. Code Availability

Our model code is written in MATLAB and is publicly and freely available (under the GPL v3 license) via GitHub at the following DOI link: <https://doi.org/10.5281/zenodo.5576789>. The reference is included in our references list, under harrison-martin, 2021. This can be updated as needed during the review process.

## 8. Video supplement

A video supplement (Supplemental Videos 1-3) is uploaded to the AV Portal of TIB Hannover under the CC BY-NC-SA 3.0 DE license. The videos can be accessed at the following DOI links:

<https://doi.org/10.5446/54887> - Martin and Edmonds Avulsion Model Supplemental Video 1

<https://doi.org/10.5446/54888> - Martin and Edmonds Avulsion Model Supplemental Video 2

<https://doi.org/10.5446/54889> - Martin and Edmonds Avulsion Model Supplemental Video 3



## 695 9. Author contribution

HM and DE conceptualized and designed the research and developed the code. HM collected and analyzed the data, wrote the manuscript, and prepared the figures. DE supervised the research and reviewed and edited the manuscript.

## 10. Competing interests

The authors declare that they have no conflicts of interest.

## 700 11. Acknowledgements

HM and DE were supported by U.S. National Science Foundation grant EAR-1911321. We would like to thank Ben Peters for assistance with preparation of Figure 1. We would also like to thank Gary Weissmann and Jeffery Valenza for helpful conversations about rivers in foreland basins.

## 12. Notation

Symbol	Name	Units
$A$	non-dimensional constant	non-dimensional
$A_{chan}$	in-channel aggradation rate at some location	meters per year
$A_{fp,f}$	fixed-rate component of overbank aggradation	meters per year
$A_{fp,tot}$	total overbank aggradation rate on the floodplain	meters per year
$A_{fp,v}$	variable-rate component of overbank aggradation	meters per year
$\alpha_A$	attraction factor	non-dimensional
$\alpha_{H,high}$	healing rate parameter for high elevations	non-dimensional
$\alpha_{H,low}$	healing rate parameter for low elevations	non-dimensional
$\alpha_R$	repulsion factor	non-dimensional





$\beta$	channel depth fraction	non-dimensional
$c_f$	drag coefficient	non-dimensional
$C_0$	bed sediment concentration	non-dimensional
$\eta_{aban,high}$	abandoned channel levee elevation	meters
$\eta_{aban,low}$	abandoned channel bed elevation	meters
$\eta_{adj,low}$	channel bed elevation for a cell adjacent to the active channel	meters
$\eta_{appr,low}$	low elevation in the cell from which a pathfinding avulsion approaches an abandoned channel	meters
$\eta_{chan,high}$	levee elevation for an active channel cell	meters
$\eta_{chan,low}$	channel bed elevation for an active channel cell	meters
$\eta_{farfield}$	elevation of a far-field floodplain cell that has never been visited by the active channel	meters
$\eta_{fp,high}$	floodplain elevation, high	meters
$\eta_{fp,low}$	floodplain elevation, low	meters
$\eta_{high,max}$	the highest active, abandoned, or floodplain high elevation in a given row	meters
$h_{aban}$	remnant depth of an abandoned channel	meters
$h_{avul}$	flow depth of the pathfinding avulsion	meters
$h_{chan}$	active channel depth	meters
$h_T$	characteristic time needed to heal one mean channel depth	years
$\bar{h}$	mean flow depth	meters



$H_{low}$	healing rate for low elevations	meters per year
$H_{high}$	healing rate for high elevations	meters per year
$L_h$	levee height above approaching floodplain	meters per year
$q$	normalized water discharge per unit basin width	square meters per year
$\rho_{sediment}$	density of sediment	kilograms per cubic meter
$\rho_{water}$	density of water	kilograms per cubic meter
$S$	sediment specific gravity	non-dimensional
$\sigma$	subsidence rate	meters per year
$t$	time	years
$T_A$	time to achieve superelevation	years
$\nu$	diffusivity	square meters per year
$x$	space	meters

### 705 13. References

- Allen, J. R. L.: Studies in fluvial sedimentation: an exploratory quantitative model for the architecture of avulsion-controlled alluvial suites, *Sedimentary Geology*, 21, 129–147, [https://doi.org/10.1016/0037-0738\(78\)90002-7](https://doi.org/10.1016/0037-0738(78)90002-7), 1978.
- Aslan, A., Autin, W. J., and Blum, M. D.: Causes of River Avulsion: Insights from the Late Holocene Avulsion History of the Mississippi River, U.S.A., *Journal of Sedimentary Research*, 75, 650–664, <https://doi.org/10.2110/jsr.2005.053>, 2005.
- 710 Assine, M. L.: River avulsions on the Taquari megafan, Pantanal wetland, Brazil, *Geomorphology*, 70, 357–371, <https://doi.org/10.1016/j.geomorph.2005.02.013>, 2005.
- Assine, M. L. and Soares, P. C.: Quaternary of the Pantanal, west-central Brazil, *Quaternary International*, 114, 23–34, [https://doi.org/10.1016/S1040-6182\(03\)00039-9](https://doi.org/10.1016/S1040-6182(03)00039-9), 2004.
- Assine, M. L., Corradini, F. A., Pupim, F. do N., and McGlue, M. M.: Channel arrangements and depositional styles in the  
 715 São Lourenço fluvial megafan, Brazilian Pantanal wetland, *Sedimentary Geology*, 301, 172–184, <https://doi.org/10.1016/j.sedgeo.2013.11.007>, 2014.
- Bernal, C., Christophoul, F., Darrozes, J., Soula, J.-C., Baby, P., and Burgos, J.: Late Glacial and Holocene avulsions of the Rio Pastaza Megafan (Ecuador–Peru): frequency and controlling factors, *Int J Earth Sci (Geol Rundsch)*, 100, 1759–1782, <https://doi.org/10.1007/s00531-010-0555-9>, 2011.



- 720 Bokulich, A.: Explanatory Models Versus Predictive Models: Reduced Complexity Modeling in Geomorphology, in: EPSA11 Perspectives and Foundational Problems in Philosophy of Science, Cham, 115–128, [https://doi.org/10.1007/978-3-319-01306-0\\_10](https://doi.org/10.1007/978-3-319-01306-0_10), 2013.
- Bridge, J. S. and Leeder, M. R.: A simulation model of alluvial stratigraphy, 26, 617–644, <https://doi.org/10.1111/j.1365-3091.1979.tb00935.x>, 1979.
- 725 Bryant, M., Falk, P., and Paola, C.: Experimental study of avulsion frequency and rate of deposition, *Geology*, 23, 365–368, [https://doi.org/10.1130/0091-7613\(1995\)023<0365:ESOAF>2.3.CO;2](https://doi.org/10.1130/0091-7613(1995)023<0365:ESOAF>2.3.CO;2), 1995.
- Buehler, H. A., Weissmann, G. S., Scuderi, L. A., and Hartley, A. J.: Spatial and Temporal Evolution of an Avulsion on the Taquari River Distributive Fluvial System from Satellite Image Analysis, *Journal of Sedimentary Research*, 81, 630–640, <https://doi.org/10.2110/jsr.2011.040>, 2011.
- 730 Burkham, D. E.: Channel Changes of the Gila River in Safford Valley, Arizona, 1846-1970, U.S. Government Printing Office, 36 pp., 1972.
- Chakraborty, T., Kar, R., Ghosh, P., and Basu, S.: Kosi megafan: Historical records, geomorphology and the recent avulsion of the Kosi River, *Quaternary International*, 227, 143–160, <https://doi.org/10.1016/j.quaint.2009.12.002>, 2010.
- Chamberlin, E. P. and Hajek, E. A.: Interpreting Paleo-Avulsion Dynamics from Multistory Sand Bodies, *Journal of Sedimentary Research*, 85, 82–94, <https://doi.org/10.2110/jsr.2015.09>, 2015.
- 735 Chamberlin, E. P. and Hajek, E. A.: Using bar preservation to constrain reworking in channel-dominated fluvial stratigraphy, *Geology*, 47, 531–534, <https://doi.org/10.1130/G46046.1>, 2019.
- Coulthard, T. J., Macklin, M. G., and Kirkby, M. J.: A cellular model of Holocene upland river basin and alluvial fan evolution, 27, 269–288, <https://doi.org/10.1002/esp.318>, 2002.
- 740 Croke, J., Fryirs, K., and Thompson, C.: Channel–floodplain connectivity during an extreme flood event: implications for sediment erosion, deposition, and delivery, 38, 1444–1456, <https://doi.org/10.1002/esp.3430>, 2013.
- Edmonds, D. A., Hajek, E. A., Downton, N., and Bryk, A. B.: Avulsion flow-path selection on rivers in foreland basins, *Geology*, 44, 695–698, <https://doi.org/10.1130/G38082.1>, 2016.
- Edmonds, D. A., Martin, H. K., Valenza, J. M., Henson, R., Weissmann, G. S., Miltenberger, K., Mans, W., Moore, J. R., Slingerland, R. L., Gibling, M. R., Bryk, A. B., and Hajek, E. A.: Rivers in reverse: Upstream-migrating dechannelization and flooding cause avulsions on fluvial fans, *Geology*, <https://doi.org/10.1130/G49318.1>, 2021.
- 745 Ethridge, F. G., Skelly, R. L., and Bristow, C. S.: Avulsion and Crevassing in the Sandy, Braided Niobrara River: Complex Response to Base-Level Rise and Aggradation, in: *Fluvial Sedimentology VI*, John Wiley & Sons, Ltd, 179–191, <https://doi.org/10.1002/9781444304213.ch14>, 1999.
- 750 Farrell, K. M.: *Sedimentology and Facies Architecture of Overbank Deposits of the Mississippi River, False River Region, Louisiana*, 1987.
- Gabet, E. J.: Gopher bioturbation: field evidence for non-linear hillslope diffusion, 25, 1419–1428, [https://doi.org/10.1002/1096-9837\(200012\)25:13<1419::AID-ESP148>3.0.CO;2-1](https://doi.org/10.1002/1096-9837(200012)25:13<1419::AID-ESP148>3.0.CO;2-1), 2000.



- Gibling, M. R., Bashforth, A. R., Falcon-Lang, H. J., Allen, J. P., and Fielding, C. R.: Log Jams and Flood Sediment Buildup  
755 Caused Channel Abandonment and Avulsion in the Pennsylvanian of Atlantic Canada, *Journal of Sedimentary Research*, 80,  
268–287, <https://doi.org/10.2110/jsr.2010.024>, 2010.
- Hack, J. T. and Goodlett, J. C.: *Geomorphology and forest ecology of a mountain region in the central Appalachians*,  
Geomorphology and forest ecology of a mountain region in the central Appalachians, United States Government Printing  
Office, Washington, D.C., <https://doi.org/10.3133/pp347>, 1960.
- 760 Hajek, E. A. and Wolinsky, M. A.: Simplified process modeling of river avulsion and alluvial architecture: Connecting models  
and field data, *Sedimentary Geology*, 257–260, 1–30, <https://doi.org/10.1016/j.sedgeo.2011.09.005>, 2012.
- harrison-martin: harrison-martin/RiverWalk: RiverWalk-AM v1.0.0, <https://doi.org/10.5281/zenodo.5576789>, 18 October  
2021.
- Hartley, A. J., Weissmann, G. S., Nichols, G. J., and Scuderi, L. A.: Fluvial form in modern continental sedimentary basins:  
765 Distributive fluvial systems: REPLY, *Geology*, 38, e231, <https://doi.org/10.1130/G31588Y.1>, 2010a.
- Hartley, A. J., Weissmann, G. S., Nichols, G. J., and Warwick, G. L.: Large Distributive Fluvial Systems: Characteristics,  
Distribution, and Controls on Development, *Journal of Sedimentary Research*, 80, 167–183,  
<https://doi.org/10.2110/jsr.2010.016>, 2010b.
- Harwood, K. and Brown, A. G.: Fluvial processes in a forested anastomosing river: Flood partitioning and changing flow  
770 patterns, 18, 741–748, <https://doi.org/10.1002/esp.3290180808>, 1993.
- Jahns, R. H.: Geologic features of the Connecticut Valley, Massachusetts, as related to recent floods,  
<https://doi.org/10.3133/wsp996>, 1947.
- Jerolmack, D. J.: Conceptual framework for assessing the response of delta channel networks to Holocene sea level rise,  
*Quaternary Science Reviews*, 28, 1786–1800, <https://doi.org/10.1016/j.quascirev.2009.02.015>, 2009.
- 775 Jerolmack, D. J. and Mohrig, D.: Conditions for branching in depositional rivers, *Geology*, 35, 463–466,  
<https://doi.org/10.1130/G23308A.1>, 2007.
- Jerolmack, D. J. and Paola, C.: Complexity in a cellular model of river avulsion, *Geomorphology*, 91, 259–270,  
<https://doi.org/10.1016/j.geomorph.2007.04.022>, 2007.
- Jones, L. S. and Schumm, S. A.: Causes of Avulsion: An Overview, in: *Fluvial Sedimentology VI*, John Wiley & Sons, Ltd,  
780 169–178, <https://doi.org/10.1002/9781444304213.ch13>, 1999.
- Khalsa, S. J. S., Borsa, A., Nandigam, V., Phan, M., Lin, K., Crosby, C., Fricker, H., Baru, C., and Lopez, L.: OpenAltimetry  
- rapid analysis and visualization of Spaceborne altimeter data, *Earth Sci Inform*, [https://doi.org/10.1007/s12145-020-00520-](https://doi.org/10.1007/s12145-020-00520-2)  
2, 2020.
- Leeder, M. R.: A Quantitative Stratigraphic Model for Alluvium, with Special Reference to Channel Deposit Density and  
785 Interconnectedness, 587–596, 1977.
- Leier, A. L., DeCelles, P. G., and Pelletier, J. D.: Mountains, monsoons, and megafans, *Geology*, 33, 289–292,  
<https://doi.org/10.1130/G21228.1>, 2005.



- Lewis, G. W. and Lewin, J.: Alluvial Cutoffs in Wales and the Borderlands, in: *Modern and Ancient Fluvial Systems*, John Wiley & Sons, Ltd, 145–154, <https://doi.org/10.1002/9781444303773.ch11>, 1983.
- 790 Mackey, S. D. and Bridge, J. S.: Three-dimensional model of alluvial stratigraphy; theory and applications, *Journal of Sedimentary Research*, 65, 7–31, <https://doi.org/10.1306/D42681D5-2B26-11D7-8648000102C1865D>, 1995.
- Makaske, B., Maathuis, B. H. P., Padovani, C. R., Stolker, C., Mosselman, E., and Jongman, R. H. G.: Upstream and downstream controls of recent avulsions on the Taquari megafan, Pantanal, south-western Brazil, 37, 1313–1326, <https://doi.org/10.1002/esp.3278>, 2012.
- 795 Martin, Harrison K.; Edmonds, Douglas A.: Martin and Edmonds Avulsion Model Supplemental Video 1, Supplemental videos of the paper "The push and pull of abandoned channels: How floodplain processes and healing affect avulsion dynamics and alluvial landscape evolution in foreland basins". <https://doi.org/10.5446/54887>
- Martin, Harrison K.; Edmonds, Douglas A.: Martin and Edmonds Avulsion Model Supplemental Video 2, Supplemental videos of the paper "The push and pull of abandoned channels: How floodplain processes and healing affect avulsion dynamics and
- 800 alluvial landscape evolution in foreland basins". <https://doi.org/10.5446/54888>
- Martin, Harrison K.; Edmonds, Douglas A.: Martin and Edmonds Avulsion Model Supplemental Video 3, Supplemental videos of the paper "The push and pull of abandoned channels: How floodplain processes and healing affect avulsion dynamics and alluvial landscape evolution in foreland basins". <https://doi.org/10.5446/54889>
- Martin, J., Sheets, B., Paola, C., and Hoyal, D.: Influence of steady base-level rise on channel mobility, shoreline migration,
- 805 and scaling properties of a cohesive experimental delta, 114, <https://doi.org/10.1029/2008JF001142>, 2009.
- Mohrig, D., Heller, P. L., Paola, C., and Lyons, W. J.: Interpreting avulsion process from ancient alluvial sequences: Guadalope-Matarranya system (northern Spain) and Wasatch Formation (western Colorado), *GSA Bulletin*, 112, 1787–1803, [https://doi.org/10.1130/0016-7606\(2000\)112<1787:IAPFAA>2.0.CO;2](https://doi.org/10.1130/0016-7606(2000)112<1787:IAPFAA>2.0.CO;2), 2000.
- Moodie, A. J., Nittrouer, J. A., Ma, H., Carlson, B. N., Chadwick, A. J., Lamb, M. P., and Parker, G.: Modeling Deltaic Lobe-
- 810 Building Cycles and Channel Avulsions for the Yellow River Delta, China, 124, 2438–2462, <https://doi.org/10.1029/2019JF005220>, 2019.
- Morón, S., Amos, K., Edmonds, D. A., Payenberg, T., Sun, X., and Thyer, M.: Avulsion triggering by El Niño–Southern Oscillation and tectonic forcing: The case of the tropical Magdalena River, Colombia, *GSA Bulletin*, 129, 1300–1313, <https://doi.org/10.1130/B31580.1>, 2017.
- 815 Moudrý, V., Lecours, V., Gdulová, K., Gábor, L., Moudrá, L., Kropáček, J., and Wild, J.: On the use of global DEMs in ecological modelling and the accuracy of new bare-earth DEMs, *Ecological Modelling*, 383, 3–9, <https://doi.org/10.1016/j.ecolmodel.2018.05.006>, 2018.
- Nanson, G. C.: Point bar and floodplain formation of the meandering Beatton River, northeastern British Columbia, Canada, 27, 3–29, <https://doi.org/10.1111/j.1365-3091.1980.tb01155.x>, 1980.
- 820 Nanson, G. C. and Croke, J. C.: A genetic classification of floodplains, *Geomorphology*, 4, 459–486, [https://doi.org/10.1016/0169-555X\(92\)90039-Q](https://doi.org/10.1016/0169-555X(92)90039-Q), 1992.



- Neuenschwander, A. L. and Pitts, K.: Ice, Cloud, and Land Elevation Satellite 2 (ICESat-2) Algorithm Theoretical Basis Document (ATBD) for Land-Vegetation Along-Track Products (ATL08), [https://nsidc.org/sites/nsidc.org/files/technical-references/ICESat2\\_ATL08\\_ATBD\\_r003.pdf](https://nsidc.org/sites/nsidc.org/files/technical-references/ICESat2_ATL08_ATBD_r003.pdf), 2020.
- 825 Neuenschwander, A. L., Pitts, K., Jelley, B. P., Robbins, J., Klotz, B., Popescu, S. C., Nelson, R. F., Harding, D., Pederson, D., and Sheridan, R.: ATLAS/ICESat-2 L3A Land and Vegetation Height, version 3, <https://doi.org/10.5067/ATLAS/ATL08.003>, 2020.
- O’Loughlin, F. E., Paiva, R. C. D., Durand, M., Alsdorf, D. E., and Bates, P. D.: A multi-sensor approach towards a global vegetation corrected SRTM DEM product, *Remote Sensing of Environment*, 182, 49–59,  
830 <https://doi.org/10.1016/j.rse.2016.04.018>, 2016.
- Paola, C., Heller, P. L., and Angevine, C. L.: The large-scale dynamics of grain-size variation in alluvial basins, 1: Theory, 4, 73–90, <https://doi.org/10.1111/j.1365-2117.1992.tb00145.x>, 1992.
- Pelletier, J. D., Mayer, L., Pearthree, P. A., House, P. K., Demsey, K. A., Klawon, J. E., and Vincent, K. R.: An integrated approach to flood hazard assessment on alluvial fans using numerical modeling, field mapping, and remote sensing, *GSA*  
835 *Bulletin*, 117, 1167–1180, <https://doi.org/10.1130/B25544.1>, 2005.
- Pizzuto, J. E.: Sediment diffusion during overbank flows, 34, 301–317, <https://doi.org/10.1111/j.1365-3091.1987.tb00779.x>, 1987.
- Pupim, F. do N., Assine, M. L., and Sawakuchi, A. O.: Late Quaternary Cuiabá megafan, Brazilian Pantanal: Channel patterns and paleoenvironmental changes, *Quaternary International*, 438, 108–125, <https://doi.org/10.1016/j.quaint.2017.01.013>, 2017.
- 840 Ratliff, K. M., Hutton, E. H. W., and Murray, A. B.: Exploring Wave and Sea-Level Rise Effects on Delta Morphodynamics With a Coupled River-Ocean Model, 123, 2887–2900, <https://doi.org/10.1029/2018JF004757>, 2018.
- Ratliff, K. M., Hutton, E. W. H., and Murray, A. B.: Modeling long-term delta dynamics reveals persistent geometric river avulsion locations, *Earth and Planetary Science Letters*, 559, 116786, <https://doi.org/10.1016/j.epsl.2021.116786>, 2021.
- Reitz, M. D., Jerolmack, D. J., and Swenson, J. B.: Flooding and flow path selection on alluvial fans and deltas, 37,  
845 <https://doi.org/10.1029/2009GL041985>, 2010.
- Roering, J. J., Kirchner, J. W., and Dietrich, W. E.: Evidence for nonlinear, diffusive sediment transport on hillslopes and implications for landscape morphology, 35, 853–870, <https://doi.org/10.1029/1998WR900090>, 1999.
- Rossetti, D. F. and Valeriano, M. M.: Evolution of the lowest amazon basin modeled from the integration of geological and SRTM topographic data, *CATENA*, 70, 253–265, <https://doi.org/10.1016/j.catena.2006.08.009>, 2007.
- 850 Schumde, T. H.: Some Aspects of Land Forms of the Lower Missouri River Floodplain, 53, 60–73, 1963.
- Slingerland, R. and Kump, L.: *Mathematical Modeling of Earth’s Dynamical Systems: A Primer*, Princeton University Press, 246 pp., 2011.
- Slingerland, R. and Smith, N.: River avulsions and deposits, *Annual Review of Earth and Planetary Sciences*, 32, 257–285, <https://doi.org/10.1146/annurev.earth.32.101802.120201>, 2004.





- 855 Smith, N., Slingerland, R., Pérez-Arlucea, M., and Morozova, G.: The 1870s avulsion of the Saskatchewan River, *Canadian Journal of Earth Sciences*, 35, 453–466, <https://doi.org/10.1139/cjes-35-4-453>, 1998.
- Sun, T., Paola, C., Parker, G., and Meakin, P.: Fluvial fan deltas: Linking channel processes with large-scale morphodynamics, 38, 26-1-26–10, <https://doi.org/10.1029/2001WR000284>, 2002.
- Toonen, W. H. J., Kleinhans, M. G., and Cohen, K. M.: Sedimentary architecture of abandoned channel fills, 37, 459–472, <https://doi.org/10.1002/esp.3189>, 2012.
- 860 Tooth, S., McCarthy, T. S., Brandt, D., Hancox, P. J., and Morris, R.: Geological controls on the formation of alluvial meanders and floodplain wetlands: the example of the Klip River, eastern Free State, South Africa, 27, 797–815, <https://doi.org/10.1002/esp.353>, 2002.
- Valenza, J. M., Edmonds, D. A., Hwang, T., and Roy, S.: Downstream changes in river avulsion style are related to channel morphology, 11, 2116, <https://doi.org/10.1038/s41467-020-15859-9>, 2020.
- 865 Weissmann, G., Hartley, A., Scuderi, L., Nichols, G., Davidson, S., Owen, A., Atchley, S., Bhattacharyya, P., Chakraborty, T., Ghosh, A., Nordt, L., Michel, L., and Tabor, N.: Prograding distributive fluvial systems: Geomorphic models and ancient examples, <https://doi.org/10.2110/sepmsp.104.16>, 1 January 2013.
- Weissmann, G. S., Hartley, A. J., Nichols, G. J., Scuderi, L. A., Olson, M., Buehler, H., and Banteah, R.: Fluvial form in modern continental sedimentary basins: Distributive fluvial systems, *Geology*, 38, 39–42, <https://doi.org/10.1130/G30242.1>, 2010.
- 870 Weissmann, G. S., Hartley, A. J., Scuderi, L. A., Nichols, G. J., Owen, A., Wright, S., Felicia, A. L., Holland, F., and Anaya, F. M. L.: Fluvial geomorphic elements in modern sedimentary basins and their potential preservation in the rock record: A review, *Geomorphology*, 250, 187–219, <https://doi.org/10.1016/j.geomorph.2015.09.005>, 2015.
- 875 Wells, N. A. and Dorr, J. A.: A Reconnaissance of Sedimentation on the Kosi Alluvial Fan of India, 14, 1987.
- Wolman, M. G. and Eiler, J. P.: Reconnaissance study of erosion and deposition produced by the flood of August 1955 in Connecticut, 39, 1–14, <https://doi.org/10.1029/TR039i001p00001>, 1958.
- Wolman, M. G. and Leopold, L. B.: River flood plains: Some observations on their formation, *River flood plains: Some observations on their formation*, U.S. Government Printing Office, Washington, D.C., <https://doi.org/10.3133/pp282C>, 1957.
- 880 Zani, H., Assine, M. L., and McGlue, M. M.: Remote sensing analysis of depositional landforms in alluvial settings: Method development and application to the Taquari megafan, Pantanal (Brazil), *Geomorphology*, 161–162, 82–92, <https://doi.org/10.1016/j.geomorph.2012.04.003>, 2012.
- Zwoliński, Z.: Sedimentology and geomorphology of overbank flows on meandering river floodplains, *Geomorphology*, 4, 367–379, [https://doi.org/10.1016/0169-555X\(92\)90032-J](https://doi.org/10.1016/0169-555X(92)90032-J), 1992.